ACS OMEGA

Open Access

http://pubs.acs.org/journal/acsodf

Review

Nanocomposite Marvels: Unveiling Breakthroughs in Photocatalytic Water Splitting for Enhanced Hydrogen Evolution

Vikash Kumar, Gajendra Prasad Singh, Manish Kumar, Amit Kumar,* Pooja Singh, Alok Kumar Ansu, Abhishek Sharma, Tabish Alam, Anil Singh Yadav, and Dan Dobrotă*

Cite This: *ACS Omega* 2024, 9, 6147−6164

Read Online

ACCESS | Metrics & More | Article Recommendations

ABSTRACT: An overview of the significant innovations in photocatalysts for H_2 development, photocatalyst selection criteria, and photocatalytic modifications to improve the photocatalytic activity was examined in this Review, as well as mechanisms and thermodynamics. A variety of semiconductors have been examined in a structured fashion, such as TiO_2-, g-C_3N_4-, graphene-, sulfide-, oxide-, nitride-, oxysulfide-, oxynitrides, and cocatalyst-based photocatalysts. The techniques for enhancing the compatibility of metals and nonmetals is discussed in order to boost photoactivity within visible light irradiation. In particular, further deliberation has been carried out on the development of heterojunctions, such as type I, type II, and type III, along with Z-systems, and S-scheme systems. It is important to thoroughly investigate these issues in the sense of visible light irradiations to enhance the efficacy of photocatalytic action. In fact, another advancement in this area may include hiring mediators including grapheme oxide and metals to establish indirect Z-scheme montages with a correct band adjustment. The potential consideration of reaction chemology, mass transfer, kinetics of reactions, restriction of light diffusion, and the process and selection of suitable light and photoreactor also will optimize sustainable hydrogen output efficiency and selectivity.

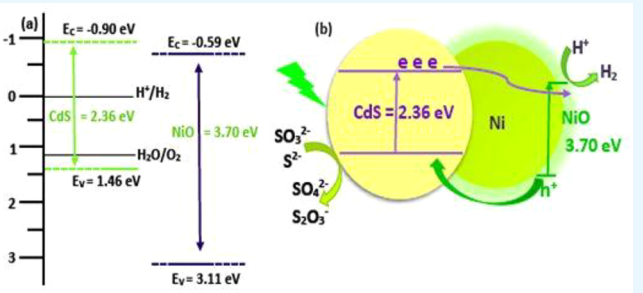

1. INTRODUCTION

Due to the exponential increase in global energy consumption and degradation of the environment due to fossil fuels, it is very necessary to enhance renewable and sustainable resources. Recently, solar energy has gained prominence as a clean and ecofriendly source of power. There exist various methods to harness solar energy, with one approach being the utilization of photocatalytic processes to split water and generate hydrogen via the conversion of solar energy. As hydrogen is a developing energy bearer, it has a high energy density without carbon content and moreover is readily transportable. Hydrogen can also discharge energy by straight ignition or in a hydrogen power module with the main side product being water. Of late, the obstacle to the acknowledgment of commercialized water splitting is the necessity to deliver hydrogen production at a focused expense contrasted with the contemporary commercial hydrogen generation procedure, including changing non-renewable energy sources. Types of solar water splitting systems are as follows: photovoltaic electrolysis (PV-E), photocatalysis, and photoelectrochemical cells (PE-Cs).[1] Photocatalytic systems are much cheaper and have a low operational cost out of the three methods of conversion. The cost of hydrogen production hinges on certain assumptions, particularly that future photocatalytic systems will achieve a solar-to-hydrogen conversion efficiency of up to 10%, a significant improvement compared to the approximately 1% efficiency observed in small-scale trials.[2,3] Given the critical role of the solar-to-hydrogen conversion efficiency in determining overall hydrogen production costs, the primary objective of this endeavor is to develop and build a highly efficient water-splitting technique.[4]

Materials in this environment the must display the properties needed to successfully achieve specific applications. In order to produce hydrogen, the photocatalytical materials require particular parameters. They are (i) adequate band edge location, (ii) a narrow energy gap band, (iii) enhanced charge separation, (iv) improved resistance to recombination, and (v) effective interfacial interlinkages.[5,6] Under these circumstances the synthesis of materials with changeable band gap energies and band edge placement has been given the main emphasis in order to generate the species needed for redox and mostly to absorb the entire energy of the sun, which is the ultraviolet−visible−near-infrared (UV−vis−NIR) sun spectrum.[7,8]

Received: October 15, 2023
Revised: January 2, 2024
Accepted: January 5, 2024
Published: January 30, 2024

Scheme 1. Solar Energy Spectrum Diagram with Wavelength Distribution

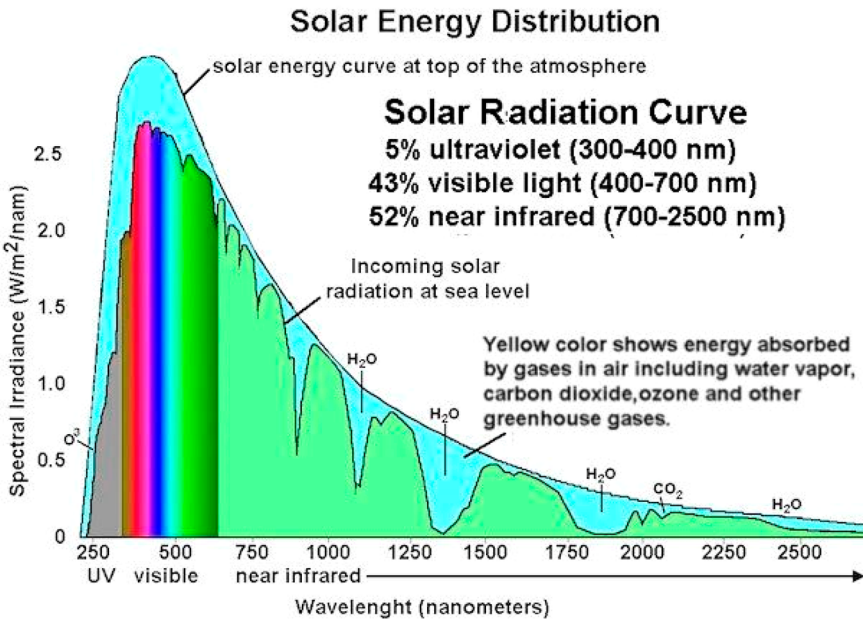

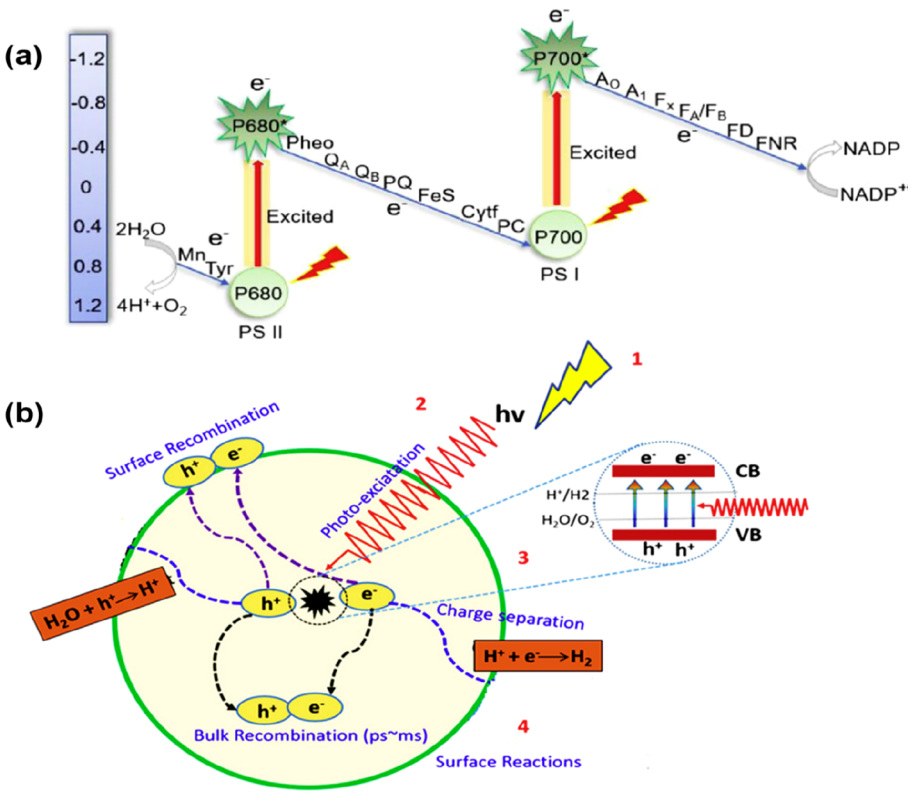

Figure 1. (a) The mechanism of charge separation in natural photosynthesis. Reprinted with permission from ref 24. Copyright 2020 Elsevier. (b) The phenomenon of charge recombination in the process of photocatalysis. Reprinted with permission from ref 25. Copyright 2015 Royal Society of Chemistry.

Though experts have acknowledged that photocatalytic components such as TiO_2 seem to be UV-powered, in later years photocatalytic materials illuminated by the sun will become more powerful in their photocatalytic usage design and implementation.[9]

The industrial-scale development of the Earth's abundant light energy source to perform photocatalytic reactions in the restraint and transferable environments. We can note that solar energy falling on earth contains 5% of UV, 45% visible and 50% NIR energies.[10] To design a photocatalyst, the band edge position of the valence band and conduction band is very important. To design a full-sunlight-driven photocatalyst, it is very daring and rousing to control both its band edge location and band gap energy.[8] Combining components with certain characteristics that can capture UV−vis−NIR energy can achieve this.[11] Besides the basic requirements of photocatalytic

https://doi.org/10.1021/acsomega.3c07822
ACS Omega 2024, 9, 6147−6164

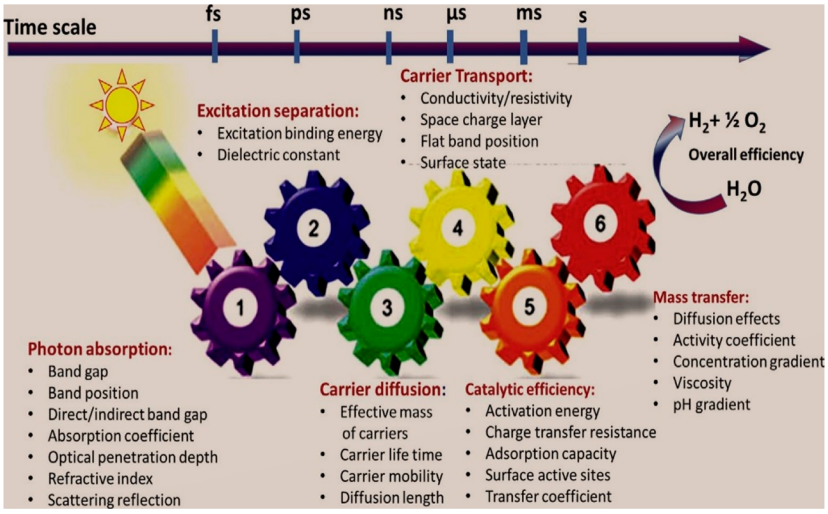

Figure 2. Schematic of important phases for the hydrogen production in the process of photocatalytic water separation. Reprinted with permission from ref 26. Copyright 2018 Royal Society of Chemistry.

activity, there is a further component known as the electron storage material (ESM) is essential to build a photocatalyst to catalyze a reaction under obscure circumstances.[12,13]

The energy requirements of the reaction have limited the semiconductor band gap. The most suitable band gap for splitting of water is 1.9−2.3 eV.[14] However, in photocatalytic processes, many of the narrow band gap semiconductors are not durable. Broad range semiconductor gaps like TiO_2 are durable but can only absorb UV light, resulting in reduced solar to hydrogen conversion rates.[15,16] One approach to this problem is to combine two different materials to produce a catalyst based on a heterojunction.

Localized surface plasmon resonance (LSPR) is formed on nanostructures decorated with a metal surface, such as Au, Ag, Al, or Cu.[17−19] Au, Ag, Al, and Cu nanoparticles (NPs) can be used as photosensitizers to tune broad absorption bands from ultraviolet to near-infrared wavelengths through LSPR to suppress the recombination of electron−hole pairs for the application of the photodetector. Thus, LSPR interacted with the piezo potential effect to catalyze the HER.[17−19,190]

The photocatalyst is the foundation stone of the photocatalysis process. The transition metal oxide and sulfide compose several hundred photocatalyst compounds. In 2009, a new age of free metal photocatalysts started with the creation of polymer carbon nitride in contrast to metal systems.[20] Metal-untied carbon nitrides, which include carbon and nitrogen, are earth-rich and affordable, whereas the majority of the metal photocatalyst is photocorrosive as a result of long-term light radiation. Polymeric carbon nitrides show excessive enlarged stability regardless of light irradiation and the pH of the solution.[21]

The overall water splitting by the photocatalyst is a thermodynamic process consisting of two half reactions to generate hydrogen and oxygen, requiring +237.2 kJ/mol free energy and 1.23 V standard reduction potential.[22,23]

There are myriad reviews in regards to overall water splitting dependent on particulate photocatalysts that have been promulgated. Here we are reviewing recent important developments in photocatalysts for water splitting hydrogen production.

2. MECHANISM FOR SPLITTING WATER AND EVOLVING HYDROGEN THROUGH PHOTOCATALYSIS

Photocatalytic water splitting is modified by a photosynthetic procedure that may be portrayed from the perspective of the photocatalyst as a synthetic response enhanced via photo-illumination. The photosynthetic process in plants is a crucial mechanism involving two photochemical processes and multiple intermediate enzyme reduction reactions. At the point when daylight falls over the plant, chlorophyll, the primary donor in photosystem II, is excited.[24] It is a huge marvel in the photocatalytic procedure, assuming crucial jobs in regards to the determination of appropriate photocatalysts for upgraded hydrogen evolution advancement. For the most part, the following advances are associated with the photocatalytic procedure: (1) light collection, (2) charge partition, (3) transport of electrons and holes outside the photocatalyst, and (4) reduction response.

The theory for the function of the photocatalytic splitting of water is composed of three components: a photocatalyst, a light source, and a water source. When exposed to light, holes generated in the photocatalyst oxidize the water in to O_2 and H^+, whereas H^+ is reduced to H_2 by photogenerated electrons. However, if electrons and holes do not necessarily reach the base, they are recombined and heat is released. In the design of photocatalysts, all phases involved in the photocatalytic process, including photon assimilation, photorecognized separation of charge, charging diffusion/transport, mass transmission, and catalytic responses on the operative location of the catalyst, are crucial to comprehend. The process of photocatalytic water splitting depends greatly on the characteristics of the photocatalyst, the cocatalyst, reaction conditions, and reactant adsorption.

Regarding the time scale, photoexcited charges rapidly reposition themselves within femto- to picoseconds to their respective bands and subsequently transport to the catalytic surface within a nano- or microsecond time frame for oxidation and reduction reactions.[26]

2.1. The Thermodynamic Aspects of the Water Splitting Process. Energetic electrons are driven to achieve internal equilibrium rather than reside near the band gap,

https://doi.org/10.1021/acsomega.3c07822
ACS Omega 2024, 9, 6147−6164

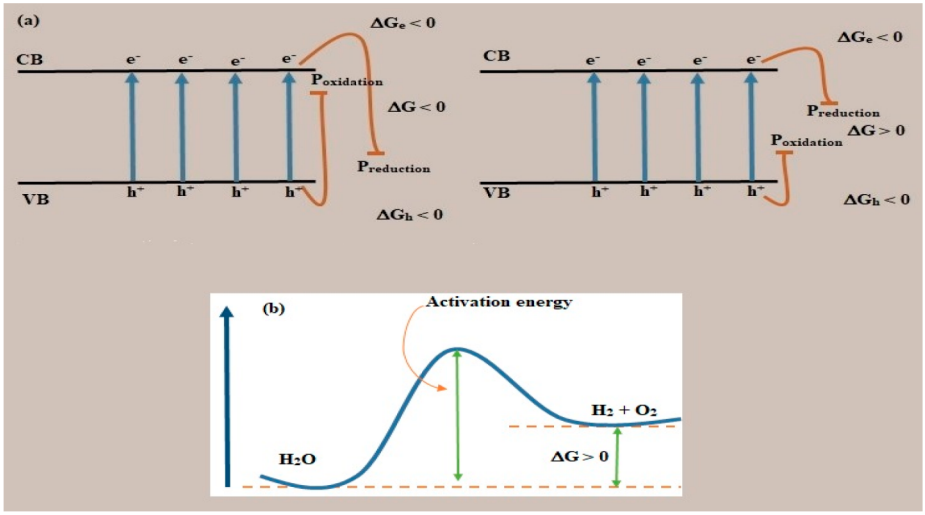

Figure 3. (a) The electronic structure of photocatalytic semiconductor and associated Gibbs energy change. (b) Splitting of water as mounting reaction. Reprinted with permission from ref 28. Copyright 2018 Wiley.

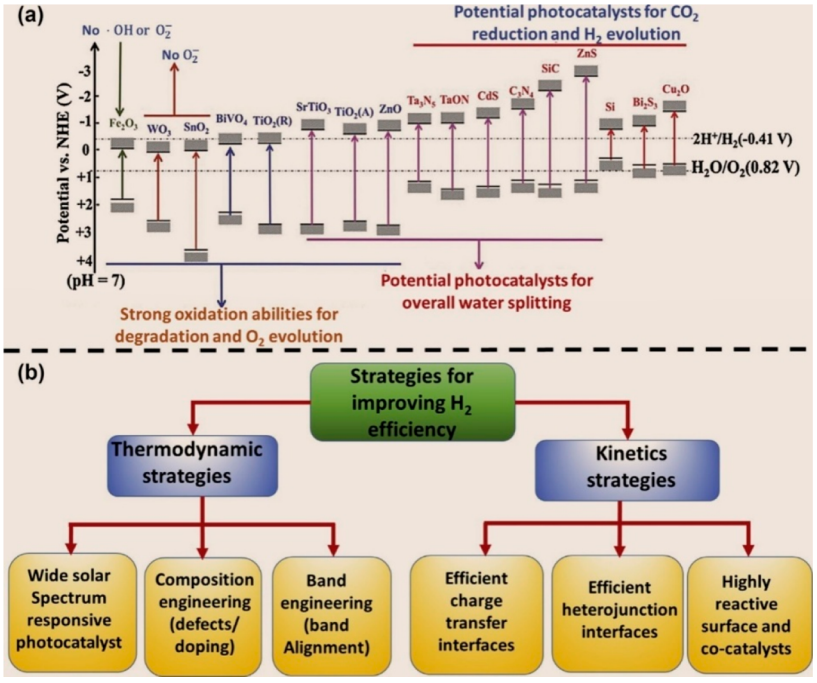

Figure 4. (a) Electronic band arrangement of certain semiconductor materials at a pH level of 7. (b) Methods for photocatalytic hydrogen production involving both thermodynamic and kinetic principles. Reprinted with permission from ref 34. Copyright 2004 Elsevier.

which is primarily because they have a shorter relaxation time within the conduction band. This state of inner equilibrium in electrons is referred to as quasi-balance states, and it corresponds to the potential of electrons and holes at quasi-Fermi levels.[27]

$$F_n = E_c + k_B T \ln \frac{n}{N_c} \quad (1)$$

$$F_p = E_v + k_B T \ln \frac{p}{N_v} \quad (2)$$

$$\Delta G = -|F_n - F_p| = -E_g - k_B T \ln \frac{np}{N_v N_c} \quad (3)$$

Here E_c and E_v are the energy level positions of the conduction band minimum and valence band maximum, respectively; k_B is the Boltzmann constant; N_c and N_v are the effective density of states of the conduction band and valence band, respectively; and n and p are concentrations of charge carriers.

The thermodynamic photoreactive driving force is proportional to the electron and hole population differential, as shown in eq 3. Figure 3(a) indicates that the reduction potential and oxidation potential disparity is referred to as the Gibbs energy transition. Water splitting is a reaction that requires energy, as illustrated in Figure 3(b). If electrons are thermodynamic ($\Delta H = 0$), ΔG is null, such that a photocatalytic reaction can be achieved without any availability of net force. This demonstrates that heat is not an impulse for electron−hole pair generation. However, the yield of photo-

https://doi.org/10.1021/acsomega.3c07822
ACS Omega 2024, 9, 6147−6164

catalytic water splitting has been reported to increase with temperature.

3. PHOTOCATALYST SELECTION FOR SPLITTING OF WATER FOR HYDROGEN EVOLUTION

3.1. Photocatalyst Recapitulation and Selection. The main element determining the choice of photocatalyst for water splitting is optimizing efficiency. In the development of photocatalysts, the following frameworks must be contemplated: valence and conduction band position, light harvesting capacities, migration of charge carriers, surface area, and photostability.[29,30] However, photocatalysts with a single component cannot meet the desired photocatalytic characteristics. The standard titanium dioxide (TiO_2) photocatalyst, for instance, suffers from a recombination of the load and a wide band gap; likewise, pure CdS has a lower band gap than TiO_2, but its efficiency is limited because of the recombination of the charges (electrons and holes).[31] After research on the synthesis of hydrogen from water under solar radiation, some more semiconductors such as ZnO, Ta_2O_5, CdSe, Fe_2O_3, SnO_2, SrTiO3, WO_2, WO_3, CuO, Cu_2O, and so forth have also been noted.[32,33]

3.2. Types of Photocatalysts. *3.2.1. Titanium Dioxide (TiO_2).* Titanium dioxide (TiO_2) nanomaterials exhibis a robust energy band configuration,[32,35,36] along with high photochemical stability.[36−38] These energized radicals and ions then engage in reactions and break down dye molecules, resulting in the production of CO_2 and water. However, TiO_2's wider bandgap (3.2 eV) limits its ability to efficiently absorb natural light radiation. Therefore, it becomes necessary to modify the TiO_2 structure to enhance its photocatalytic efficiency. Numerous efforts have been undertaken to improve TiO_2's photocatalytic capabilities, including methods such as cation or anion doping, the addition of extra layers, and the creation of heterostructural hybrids. TiO_2 is an inorganic semiconductor with the well-known form of the n type. It can then be used to shape a p−n heterojunction arrangement with a p-type semiconductor like p-Si, which accelerates movement of the electrons from p-Si to active positions.

3.2.2. Other Metal Oxides. Several types of metal oxides are commonly used as water splitting photocatalyst materials, such as, for instance, ZnO, WO_3, Fe_2O_3, CuO and so forth.[39] ZnO contributes to fast photogenerated recombination of charges and thus poor performance induced by its photocatalytic activity. WO_3, on the contrary, is a stable O_2 generation photocatalyst in light radiation; notably, however, no H_2 evolution is noticed at speed because of its narrow conduction band. Meantime, Fe_2O_3 is not very stable and has the same problem as WO_3. Copper oxide (CuO), having a low bandgap of 1.4 eV, is among the principal p-type semiconductors and has been used for photoconducting and photochemical purposes in solar cells.[40−42] CuO is commonly used as a photocatalyst sensitizer, as when CuO is used alone as a photocatalyst it is unable to achieve sufficient photocatalytic activity.[43,44]

3.2.3. Metal Nitrides. Metal nitride is known as a clear potential H_2 production, O_2 analysis, and CO_2 removal photocatalyst and has exclusion from clear processing to contaminants. The electronic configuration of this visible-light photocatalyst exhibits a limited surface area and an elevated rate of charge recombination.[45] For this reason, it is essential to enhance the photocatalytic characteristics of g-C_3N_4 in a visible light source with various functional groups in order to overcome these anomalies.[46,47] β-$Ge_3N_4$is a metal nitride that acts photocatalytically and is likely to function as a possible photocatalyst when RuO_2 is spread on a nitride surface as a photocatalyst for the evolution of H_2 and O_2.[48]

3.2.4. Metal Sulfides. Metal sulfides are also known as forward-looking photocatalyst candidates that respond clearly to light. The sulfide valence band generally consists of S 3p orbitals, leading to a more adverse and smaller range than metal oxides. Yet, when it comes to photocatalysts, the question of photocorrosion is a typical problem for most metal sulfides. ZnS is a convenient photocatalyst for the production of H_2 ,but it corresponds to the UV light in its 3.6 eV bandgap. In the absence of sacrificial donors, it experiences photochemical decomposition into components.[49] However, it is unstable at negative conduction band potentials because of its corrosion behavior. The construction of a heterojunction with an appropriate electronic interface arrangement is, therefore, certainly an effective means of recognizing the separation of photoinducing charge carriers. WS_2 and $CuInS_2$ have been reported as metal sulfide photocatalysts, but their H_2 evolution efficiency is quite low when used as single materials.

3.2.5. Oxysulfides and Oxynitrides. In comparison to oxide families, two hardly investigated materials contain metal oxynitrides and oxysulfides. They have a wide range of adjustable band gaps from semiconductors to metals. As a result, their conductivity properties vary by structure. These are more covalent than metal oxides and thus, in comparison to metals, are not easily oxidized. Due to their robust half reactions in H_2/O_2 and the absorption of O in the visible region, they were considered to be very good photocatalysts in water splitting is due to their substitution with low-negativity N or S atoms.[50] The valence bands of oxysulfides like Sm_2−$Ti_2S_2O_5$ and oxynitrides like TaON consist primarily of blended N 2p (S 3p) and O 2p orbitals, although there are vacant N or S d orbitals as basic elements of the valence band.

A photoelectrochemical (PEC) cell, constructed using Al-doped $La_5Ti_2Cu_{0.9}Ag_{0.1}S_5O_7$ (Al-LTCA) and $BaTaO_2N$ (BTON) photoelectrodes fabricated via particle-transfer (PT) methods, demonstrates the potential for spontaneous overall water splitting under visible light, accompanied by a notably high Faradaic efficiency.[184] The favorable attributes of the Al-LTCA photocathode, such as its long absorption edge wavelength and positive onset potential, contribute to its effectiveness in spontaneous PEC water splitting when combined with photoanodes possessing extended absorption edges, such as BTON, $BaNbO_2N$, and Ta_3N_5. Despite these advantages, the observed photocurrent in the PEC cell falls below expectations. A primary factor contributing to this lower photocurrent is attributed to the use of a suboptimal electrolyte, as the pH 11 aqueous sulfate solution utilized in the PEC cell is not ideal for both photoelectrodes.

It is worth noting that while an Al-LTCA photocathode may exhibit a relatively high photocurrent in a mildly alkaline aqueous sulfate solution, this photocurrent significantly decreases in strongly alkaline aqueous phosphate solutions. In contrast, a BTON photoanode demonstrates a comparatively substantial photocurrent in strongly alkaline aqueous phosphate solutions.

$La_5Ti_2CuS_5O_7$ is used with the goal of fashioning photocatalysts responsive to visible light and boasting extended absorption edge wavelengths. Through a solid-state reaction, $La_5Ti_2Cu(S_{1-x}Se_x)_5O_7$ ($LTCS_{1-x}Se_xO$) solid solutions were synthesized across the composition spectrum of $0 \leq x \leq 1$, and

https://doi.org/10.1021/acsomega.3c07822
ACS Omega 2024, 9, 6147−6164

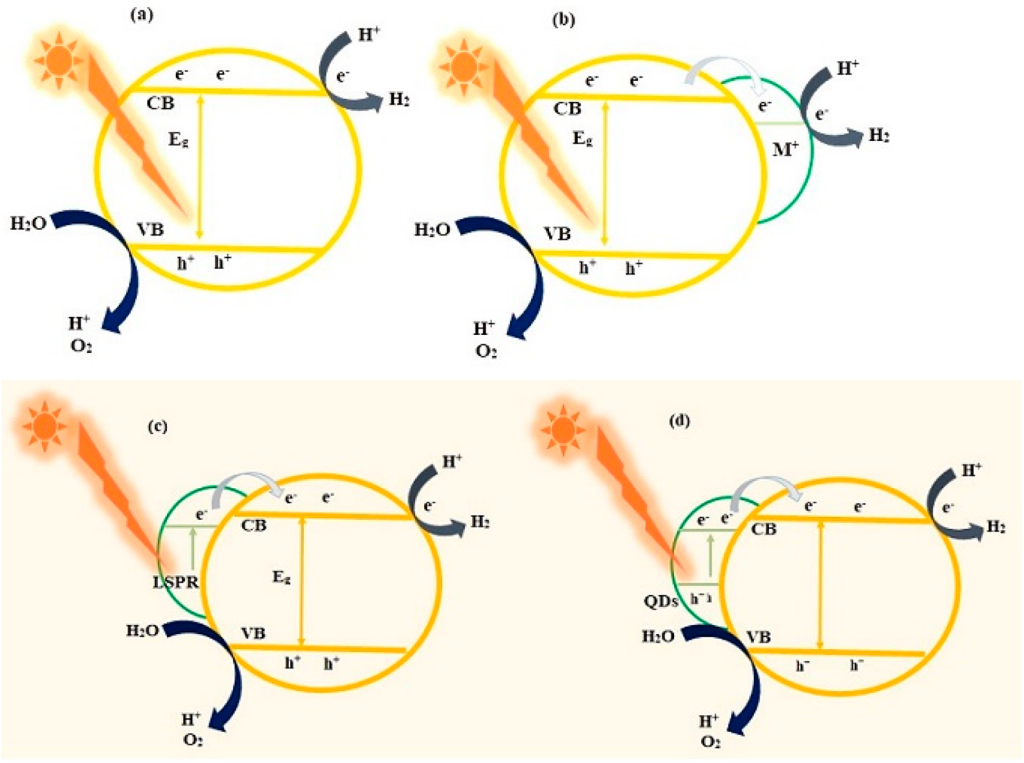

Figure 5. Various surface treatments aimed at achieving visible light absorption and the separation of charge carriers can be categorized as follows: (a) the semiconductor alone, (b) a semiconductor with a Schottky contact to a metal, (c) a semiconductor modified with plasmonic metals, and (d) a semiconductor modified with quantum dots. Reprinted with permission from ref 75. Copyright 2020 Elsevier.

their physical characteristics, as well as their efficacy in the photocatalytic H_2 evolution reaction in aqueous solutions, were scrutinized.[185]

Analyzing the structural refinements disclosed that the $LTCS_{1-x}Se_xO$ series adhered to Vegard's law, with lattice constants and cell volumes exhibiting systematic changes. As the Se^{2-} content increased, the absorption edge of $LTCS_{1-x}Se_xO$ consistently shifted toward longer wavelengths, reaching a peak at 820 nm for LTCSeO ($x = 1$). Notably, $LTCS_{1-x}Se_xO$ with lower Se^{2-} concentrations displayed comparatively heightened H_2 evolution. For instance, the sample with $x = 0.2$ produced H_2 under visible light with wavelengths surpassing 640 nm, a feat not achieved by LTCSO.[186,187]

3.2.6. Cocatalyst. Finding a photocatalyst that satisfies all criteria for efficient hydrogen and oxygen production is challenging. An effective approach is critical to the development of integrated photocatalyst cocatalysts with enhanced conversion efficiencies that can separate photogenerated electron−hole pairs.[51−55] Noble metals are used in particular as efficient cocatalysts in the manufacture of photocatalytic responses.[56,57] The most commonly used cocatalysts are noble metals (Pt, Pd, Au, Ru, Rh, Co, Ni, Mo, and W) and the most common metal oxides (NiO and RuO_2).[58,59] Non-noble metal cocatalysts like alloys, phosphides, nitrides, sulfides, and carbides have been studied to increase the photocatalytic generation of hydrogen.[60−64] The photocatalyst packs the precious metal onto the surface, and photogenerated electrons migrating to the photocatalyst's surface are captured by the noble metal cocatalyst due to its lower Fermi energy level compared to that of the semiconductor photocatalyst.[65,66]

Essential for maximizing efficiency in the process of photocatalytic and photoelectrochemical (PEC) water splitting, the presence of suitable cocatalysts is paramount.[67,68] These cocatalysts play a crucial role by providing active sites for reduction or oxidation, catalyzing surface reactions through the reduction of activation energies, capturing charge carriers, and preventing the recombination of photogenerated electrons and holes.[69] Elements like noble metals, transition metal oxides, and sulfides can function as cocatalysts for either reduction or oxidation in photocatalytic reactions.[191]

In essence, a well-designed photocatalyst should encompass three fundamental functionalities: light harvesting (as a semiconductor) and dual cocatalysts for both reduction and oxidation reactions. The effectiveness of a cocatalyst relies on its compatibility with semiconductors in terms of energy levels and electronic structures. This entails having a harmonious lattice and electronic structures with suitable Fermi levels or band gaps, facilitating the right direction of charge transport processes between the semiconductor and cocatalysts driven by the built-in electric field at the interface.

Comparatively, the water oxidation half reaction poses greater challenges, both thermodynamically and kinetically, making it the rate-determining step for most water splitting photocatalysts. To overcome these challenges and achieve highly efficient overall water splitting, the search for more efficient cocatalysts for water oxidation is imperative. Notably, oxidation cocatalysts play a crucial role in safeguarding light-harvesting semiconductors, such as CdS, from photocorrosion, which is a critical issue, particularly for semiconductors with narrow band gaps like oxynitride and oxysulfide.[192]

https://doi.org/10.1021/acsomega.3c07822
ACS Omega 2024, 9, 6147−6164

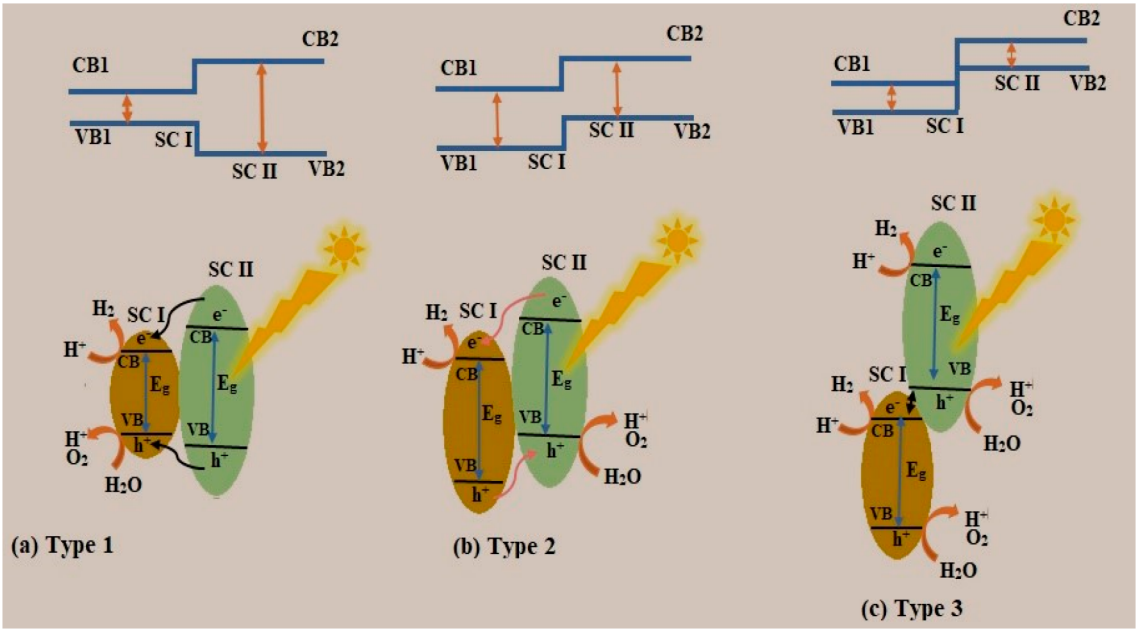

Figure 6. Scheme presenting several forms of heterojunctions for the production of photocatalytic hydrogen: (a) mounting gap heterojunction, (b) lurched gapheterojunction, and (c) fragmented gapheterojunction. Reprinted with permission from ref 78. Copyright 2017 Wiley.

4. STRATEGIES FOR IMPROVING THE PHOTOACTIVITY OF PHOTOCATALYSTS

4.1. Surface Refinement. Multiple methods are utilized on the semiconductor material surface to enhance the separation of charge carriers; these are band gap engineering, regulation of defects, surface plasmon resonance (SPR) impact, and surface refinement.[70] A pure semiconductor has no sink to capture electrons, so the charges generated will automatically recombine, making it feasible for photocatalytic processing to use just a limited portion of the carrier. The arrangement of the band gap and the presence of surface defects can modify the response to visible light and the process of separating charge carriers.[71] The difference between the higher work function of the metal and that of the semiconductor allows the development of a Schottky barrier, resulting in increased H_2 production efficiency. The efficacy of a semiconductor is improved through the transfer of electrons from the semiconductor conduction band into the metal, and the hole of the semiconductor in the valence band is left behind. This occurs when the Fermi level of metals is less than the semiconductor conduction band energy.[72] The heavy SPR influence of noble metals such as Au, Ag, and Pt improves visible light absorption and the isolation of charge carriers. The SPR effect causes hot photogenerated electrons under visible light radiation and is transferred to the conduction band of a semiconductor. Eventually, semiconductor electrons are used on the semiconductor surface to reduce H^+ for H_2 evolution.[73] Quantum dots and organic dyes enhance the absorption of visible light and enable the semiconductor to utilize visible light for the generation of electrons in the conduction band, thereby facilitating efficient hydrogen evolution.[74] Noble metals are frequently employed to enhance visible light absorption through the SPR effect and to isolate charge carriers within a semiconductor. By and large, plasmonic metals loaded into a semiconductor may act to increase the visible radiation absorption of a semiconductor as an electron sink and through photorefinement. Au supplies SPR effects, while silver metal promotes charge carrier isolation.[75,76] Therefore, maximizing the H_2 evolution by the synergistic functioning of two different metals is more likely in comparison with the single metal loading process. Enhancements made to a semiconductor with an inappropriate band structure are impractical, as they cannot be utilized, and the reactions for oxidation and reduction remain ineffective. In these conditions, the formation of heterojunction semiconductors integrated with surface refinement is a promising way of maximizing water splitting H_2 evolution.

4.2. Heterojunction Emergence. A semiconductor may also improve its photocatalytic activity by creating a heterotransition, which could improve visible light assimilation, bending the band and development of inner electric field and thus dramatically improving photocatalytic behavior by preferential band arrangement and structural charge isolation.[77] Semiconductors have the capability to form three distinct types of heterojunction structures depending on their band alignment: spanning gap, shifted gap, and fractured gap.[78,79] In the case of a staggered gap heterojunction, semiconductor II has a less favorable conduction band compared to semiconductor I, while semiconductor I has a more favorable valence band than semiconductor II.[80]

4.3. Z-Scheme Heterojunction System. With the Z-scheme, a proper shuttle redox mediator satisfies the blend of both photocatalysts. The shuttle redox mediator is a pair of acceptors and donors that helps the Z-scheme with two dissimilar photocatalyst varieties that are not in direct physical contact.[81−83] Such redox mediators are IO^{3-}/I^-, NO^{2-}/NO^{3-}, Fe^{2+}/Fe^{3+}, and Co^{2+}/Co^{3+}. When the light is irradiated, a response in the photosystem for both H_2 and O_2 occurs. Redox mediators play a key role in transferring electrons from O_2 to H_2-generating photocatalysts. However, the concurrent evolutionary responses for H_2 and O_2 are difficult because of the reverse reaction.[84] The reverse reaction happens when the acceptor and the donor are able to react with light-produced electrons, thereby decreasing the photocatalyst's quantities of agitated electrons and holes. Semiconductor I and semi-

https://doi.org/10.1021/acsomega.3c07822
ACS Omega 2024, 9, 6147−6164

conductor II at the interface include a photocatalytic Z-scheme arrangement utilizing a solid electron mediator.[85,86] Hence, a Z-scheme system builds a heterojunction system to obtain more adverse conduction band and more favorable valence band depending on the band positions of the conduction band and valence band for competent oxidation and reduction reactions. The efficiency of the Z-scheme system using mediators and metal loading, which acts as a Schottky bridge for the charge carrier separation, will further improve. Due to their excellent visible light harvesting ability and the band positionin,g oxynitride semiconductors reduce H^+ and show good stability in aqueous solutions, making them promising candidates for H_2 evolution photocatalysts in Z-scheme systems.

4.4. S-Scheme Photocatalyst Systems. Confronting the challenges outlined above, researchers have actively sought to propose an illustrative mechanism that effectively facilitates the charge transfer process in heterojunction photocatalysts. The forefront contender in this endeavor is the S-scheme heterojunction, which not only addresses the limitations inherent in the type II heterojunction system but also provides a streamlined mechanism to unravel the intricacies of charge transfer pathways in heterojunction photocatalysts. A pivotal moment in this trajectory occurred in 2019 when Yu and collaborators introduced the S-scheme heterojunction. This groundbreaking concept successfully surmounted the challenges associated with compromising the redox ability in type-II heterojunctions while upholding commendable activity levels.

As visualized in Figure 7a and b, the S-scheme heterojunction system ingeniously merges two n-type semiconductors with meticulously staggered band configurations. The oxidation photocatalyst is strategically positioned with a more positively inclined valence band, while the reduction photocatalyst boasts a conduction band with a more negative orientation. In the absence of light, electrons from the reduction photocatalyst (RP) autonomously migrate and accumulate on the adjacent oxidation photocatalyst (OP), as shown in Figure 7a. This results in positive charges being left on the RP due to the higher Fermi level of the latter. Upon achieving Fermi level equilibrium between RP and OP, the region near OP becomes negatively charged, gaining electrons, while the area near RP becomes positively charged. Consequently, this establishes an interfacial electric field (IEF) at the interface, directing the flow from RP to OP.[189]

Under the influence of light, as portrayed in Figure 7b, this IEF orchestrates the guided accumulation of photogenerated electrons and holes on the RP and OP, respectively. This orchestrated spatial separation of photogenerated electrons and holes sets the S-scheme heterojunction photocatalysts apart from their type II counterparts, showcasing their optimized redox capability.[189] The unique attributes of the S-scheme heterojunction, promising heightened photocatalytic performance, have spurred extensive research exploring various combinations of oxidation photocatalysts (OPs) and reduction photocatalysts (RPs).

4.5. Photocatalysts Using Titanium Dioxide as a Base Material. Since TiO_2 is nontoxic and cost-effective and exhibits high photostability, it serves as an excellent semiconductor material for photocatalysis.[87] However, despite these advantages, TiO_2 has three primary limitations. First, the recombination of charge carriers hinders surface reactions, leading to a low energy conversion efficiency. Furthermore,

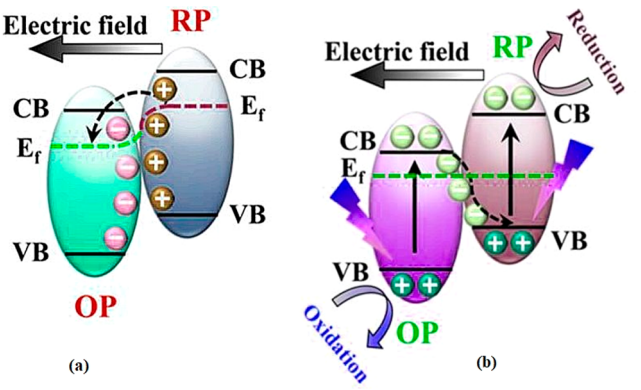

Figure 7. (a) S-scheme system in the dark. (b) S-scheme system under light irradiation. Reprinted with permission from ref 189. Copyright 2022 Elsevier.

backward reactions arise immediately as hydrogen and oxygen are mixed to create H_2O. Third, TiO_2 is a UV-active catalyst and cannot utilize the entire spectrum of the solar system. TiO_2 has a wider band gap, and it is UV irradiation-active. Because visible light is a large part of solar irradiation, this limits the photocatalyst's H_2 evolution application. There are several modifications to increase the H_2 production efficiency of TiO_2. Several approaches to improving the efficiency of TiO_2 include adding a scavenger, adding carbonate salts, dye sensitization, as well as constructing composites with TiO_2. The donor of the electron in sacrificial form will help minimize recombination of the charge carrier, as the photogenerated hole in the valence band would react with additional electrons, boosing the isolation of electron−holes and increasing quantum efficiency.[88−90] However, this approach has a drawback, as electrons provided by sacrificial agents can be depleted throughout the entire reaction.[91−95] To mitigate this issue, the addition of carbonate salts is employed to limit the reverse reaction, thereby promoting hydrogen production.[96−101]

4.6. Metal and Nonmetal Doping in TiO_2. The use of metal and nonmetallic doping elements in TiO_2 principally helps to modify its characteristics to keep electrons and holes from recombining. Metal doping mainly changes the energy level of the band gap, making it active with visible light. The constraint on charge recombination resulting from nonmetal doping arises from the formation of oxygen vacancies.[102] For instance, within TiO_2 doping, various metals and nonmetals, such as platinum, gold, copper, vanadium, carbon nanotubes (CNTs), iron, tin, carbon, nitrogen, and sulfur, have been referenced.[103,104] TiO_2's band gap decreased to 2.2 eV with nitrogen and sulfur doping, thus retaining the correct band gap for redox reaction startup.[105] The hydrothermally synthesized bromine- and chlorine-doped TiO_2 leads to extra narrow band gaps for more visible light absorption.[106]

For metal doping, sol−gel techniques, photoreduction processes, and hydrothermal processes are typical methods.[107] The introduction of copper-doped TiO_2 resulted in a heightened rate of hydrogen evolution in comparison to unadulterated TiO_2. This enhancement can be ascribed to the effective separation and transfer of charges, facilitated by the Schottky interaction between copper and TiO_2. Furthermore, TiO_2 not only possesses limited active regions for hydrogen evolution but also contains active sites where metals function as cocatalysts to facilitate the reduction reaction of hydrogen

https://doi.org/10.1021/acsomega.3c07822
ACS Omega 2024, 9, 6147−6164

evolution. In another case, C/Pt/TiO_2 synthesis reveals that the efficient transfer of charges increased the photocatalytic activity and C as a cocatalyst led to surface enhancement that induced more active areas.[108]

The surface plasmon resonance effect is another technique generated by doping metals like (Ag, Au, and Cu) onto the TiO_2. The SPR phenomenon arises when metal nanoparticles are exposed to radiation at their plasmonic resonance frequency, resulting in the creation of a potent local electric field in the vicinity of the metal surface.[109] This produces moving electrons and holes to facilitate the photocatalytic reactions. The progress of H_2 and Ag-TiO_2 under UV as well as visible light irradiation, along with their impressive performance attributed to the establishment of the Schottky barrier, is noteworthy, and effective TiO_2-Ag and Ag SPR-influenced electron transport has been reported.[110] Due to the enriched TiO_2 visible light excitement via the Au SPR effect, more electrons were transferred from Au metal on to the surface of the TiO_2, and the production of H_2 by doped Au-TiO_2 deemed threefold higher than that of Pt-TiO_2.[111] Table 1 summarizes the recent study on photocatalytic splitting of hydrogen production by means of modified TiO_2 photocatalysts for metals and nonmetals.

5. METAL OXIDE-BASED PHOTOCATALYSTS AND THEIR IMPROVEMENTS

5.1. Zinc Oxide (ZnO). ZnO has a 3.37 eV direct wide band gap and is an exciting 60 meV binding energy.[113,114] Although ZnO may not exhibit the same level of photocatalytic effectiveness as TiO_2, it is still acknowledged for its notable attributes, including high electron mobility, excellent thermal stability, cost-effectiveness, nontoxic nature, robust oxidation capabilities, significant surface-to-volume ratio, environmentally friendly characteristics, and the potential to form well-defined crystals. As a result, ZnO remains a promising semiconductor.[115−118] Due to its limited active site and the possibility of photocorrosion, the performance of ZnO is restricted.[119−124] Composites formed using another material with pure ZnO can increase the photocatalytic hydrogen production. Federal doping of metals such as Au will further boost the photocatalytic function of ZnO.[125−128] Photocorrosion is not present in gold, and it can be firmly grounded as a noble metal on surfaces. Furthermore, it demonstrates a characteristic plasmonic effect on its surface within the visible spectrum due to the collective stimulation of electrons within the gold nanostructure.[129,130]

Regarding hydrogen generation, ZnO-f proved to be the most consistent due to its morphology and heightened efficiency in absorbing light. The photocatalytic performance is further improved by loading Au on ZnO-f. Likewise, CuO-Cu_2O/ZnO has been reported for hydrogen production with improved photocatalytic activity via an interfacial charge carrier for Z-scheme systems.[131−135] A ZnO/CdS photocatalyst exhibited improved production of H_2. Enhanced photocatalytic activity is a result of the Z-scheme heterojunction formed with floral structures, which effectively separates charge carriers.

5.2. Tungsten Trioxide (WO_3). WO_3's energy band gap is relatively low, i.e. 2.6 eV, making it a reactive photocatalyst under visible light.[136,137] WO_3 has a valence band potential that is near the valence band potential of TiO_2, but WO_3 does not work efficiently because the conduction band level of WO_3 is small and limits its ability to react effectively to the surface redox.[138,139] A downside of lowering the conduction band of WO_3 so that it promotes swift recombination of the electron−hole pair produced, ultimately resulting in reduced efficiency of photocatalytic activity.[140] Photocatalytic reactions have been limited by the WO_3 photocatalyst. Researchers are currently focused on and dedicating considerable effort to enhancing the photocatalytic performance of WO_3. This involves making modifications like incorporating metals into WO_3 and establishing connections between WO_3 and various other semiconductors.[141] Several composites of WO_3, like Pt/Au/WO_3, CdS/WO_3, G-C_3N_4/WO_3, and TiO_2/WO_2, have been explored for improved photocatalytic water splitting.[142−145]

One significant approach to boosting photocatalytic activity is achieved by altering WO_3 through the incorporation of TiO_2. When WO_3 is mixed with TiO_2, WO_3 takes on the role of an electron acceptor, which aids in the transfer of electrons from TiO_2 to WO_3. This extends the interfacial charge duration, leading to improved hydrogen production. Additionally, when modified WO_3 is paired with TiO_2, the surface of the photocatalyst becomes more acidic due to the presence of monolayer of WO_x particles on TiO_2. This arrangement leads to an increased absorption of hydroxyl groups on the surface, subsequently enhancing the rate of reduction reactions for hydrogen evolution.[144] WO_3 is a successful photocatalyst that can be joined to more specifically. Many ultraviolet semiconductors, notably AgCl, ZnO, and TiO_2, are triggered under visible light with quicker separation of the load carriers and an adjustable band configuration for a more favorable valence band and more unfavorable conductive band. Thus, photocatalytic H_2 evolution by WO_3 is notably increased under visible light and can be used in the application of solar energy.

Table 1. Metals and Nonmetal Doping in TiO_2 for Photocatalytic H_2 Evolution

metal/nonmetal doping	source of light	H_2 production	refs
Pt/TiO_2	250 W iron halogenide mercury arc lamp with 37 mW cm^{-2} intensity	18.6 mmol g^{-1} h^{-1}	61
Au/TiO_2	250 W Iron halogenide mercury arc lamp with 37 mW cm^{-2} intensity	13.3 mmol g^{-1} h^{-1}	61
Co/TiO_2	300 Xe lamp	1080 μmol h^{-1}	75
NiO/TiO_2	300 W Xe lamp with 25 mW cm^{-2} intensity	337 μmol h^{-1}	76
Ta-TiO_2, Pt/Cr	visible light greater than 420 nm	11.7 μmol h^{-1}	77
TiO_2/ Pt-CdS	500 W Hg lamp (visible light)	3.7 mL	78
Fe/TiO_2	500 W halogen lamp with 368 mWm^{-2} intensity	4.9 mL	79
RhB-Co/TiO_2	300 W (O_3-less Xe lamp)	227 μmol h^{-1}	80
Ag_2O/TiO_2	solar light irradiation with 19.03 mW cm^{-2} intensity	67 μmol h^{-1}	81
Ag/TiO_2	250 W (Fe halogenide Hg lamp)	1.17 mmol g^{-1} h^{-1}	61
TiO_2-N	150 W xenon lamp solar	28 μmol h^{-1}	82
TiO_2/Ru	16 W black-light tubes with 0.8 mW cm^{-2} intensity	71.67 μmol h^{-1}	83
TiO2/Rh	16 W black-light tubes with 0.8 mW cm^{-2} intensity	10.2 μmol h^{-1}	84
CuS/TiO_2	500 W Xe lamp	111 μmol h^{-1}	85
V-TiO_2	visible light irradiation	100 μmol h^{-1}	86

https://doi.org/10.1021/acsomega.3c07822
ACS Omega 2024, 9, 6147−6164

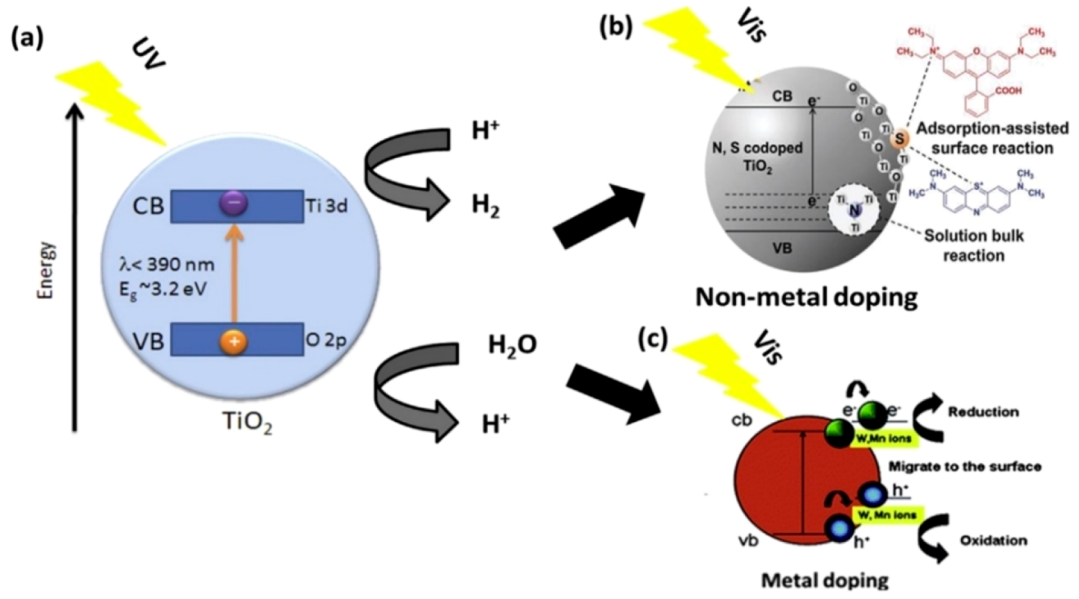

Figure 8. (a) TiO_2 band gap structure. (b) TiO2 doping with nonmetals (N and S). (c) Metal doping (W and Mn) in TiO_2. Reprinted with permission from ref 112. Copyright 2017 Elsevier.

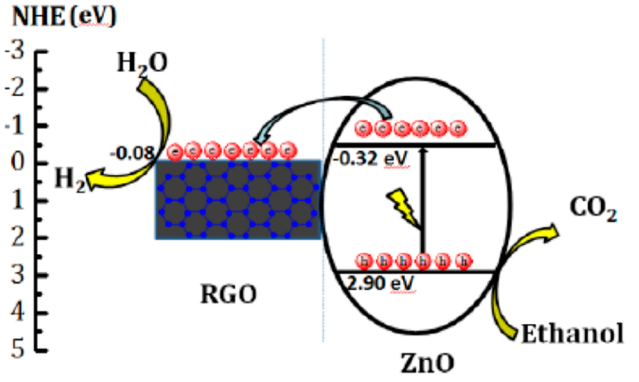

Figure 9. Schematic diagram for the charge transfer process in RGO/ZnO nanocomposites. Reprinted with permission from ref 75. Copyright 2020 Elsevier.

Table 2. ZnO-Based Photocatalysts for H_2 Evolution

materials	source of light	H_2 production	refs
Cu/ZnO	Xe lamp with cutoff >420 nm	1932 μmol h^{-1}	118
Pt/TiO_2−ZnO	400 W mercury arc lamp	2150 μmol g^{-1} h^{-1}	119
Au/ZnO-f	UV−visible irradiation (λ= 300 nm)	427 μmol g^{-1} h^{-1}	10
Graphene/ZnO	UV light	89 μmol g^{-1}	120
r-GO/ZnO	300 W xenon lamp	610 μmol g^{-1} h^{-1}	121
Cu_2O@ZnO	300 W Hg lamp	236.3 μmol	122
ZnO/CdS	300 W halogen lamp with 135 mW cm^{-2} intensity	6.18 μmol h^{-1}	123

5.3. Iron Trioxide (Fe_2O_3). Hematite is yet another excellent solar water separation photocatalyst with a corresponding band gap, which can be filled with charge excitation and separation in visible light irradiation. Fe_2O_3 is a leading photocatalyst for H_2 production, having 12.7−16.8% conversion efficiency with bad gap 2.0 eV.[146,147] Fe_2O_3's poor photocatalytic efficiency is due to its high resistance and small diffusion lengths of excitation from 2 to 20 nm.[148−151] The small aperture diffusion distance results in Fe_2O_3 absorbing light only up to 20 nm long, with less hydrogen evolution. Fe_2O_3 moderation improves the performance of photocatalytic water splitting. For example, composite TiO_2 and WO_3 formations and doping with Mo, Cr, Sn, Au, and Pt can be implemented to modify Fe_2O_3.[152] In another case, a heterojunction of grading Fe_2O_3/TiO_2 exhibited a H_2 evolution rate of 217.6 μmol h^{-1} due to the synergistic and morphological compositional effects.[153,154] The α-Fe_2O_3/$Zn_{0.4}Cd_{0.6}S$ Z-scheme heterostructure exhibited impaired charge recombination and demonstrated efficient H_2 evolution in visible light with a quantum efficacy of 11.2%.[155] Similarly, the electron transfer from Fe_2O_3's CB to Cu_2O's VB through rGO as a mediator encouraged H_2 production in the case of a rGO-Cu_2O/Fe_2O_3 composite. Due to the substantial transfer of electrons from CdSe and ZnS to Fe_2O_3, electron−hole pair recombination is decreased, which leads to effective H_2 production. Z-scheme α-Fe_2O_3/g-C_3N_4 has shown higher efficiency in hydrogen evolution under visible light than pure Fe_2O_3 due to its enhanced visible light activity, α-Fe_2O_3 facet,[110] quantum size outcomes, increased facet area, and efficient transmission and electron detachment.[133] From these we can infer that Fe_2O_3 is an encouraging visible binary light semiconductor that can be accelerated through the coupling of heterojunction with other semiconductive systems and can be used in many applications of solar energy.

5.4. Cupric Oxide and Cuprous Oxide (CuO and Cu_2O). As photocatalysts for hydrogen generation, CuO and Cu_2O are more negative than the hydrogen generation potential −0.2 V and −0.7 V, respectively, since the conduction band edges of both materials are more negative.[156−158] CuO is a p-type semiconductor that has a 1.2−1.3 eV indirect band gap, meaning that it can theoretically generate a photocurrent up to 35 mA cm^{-2}. The Cu_2O is a semiconductor p-type with 2 eV band gap and hence it has a theoretical photocurrent of 14.7 mA cm^{-2} in normal air mass 1.5 radiation.[135] It can absorb visible light in comparison with conventional photocatalysts like TiO_2, which only absorbs UV

https://doi.org/10.1021/acsomega.3c07822
ACS Omega 2024, 9, 6147−6164

light. In contrast to Cu_2O, the utilization of CuO for the purpose of producing H_2 through photocatalytic water splitting is significantly limited.[159−161] However, CuO has been used as a hydrogen production cocatalyst as the active material in solar cells, as well as in practical nanostructures and nanocomposites in many papers.[162−166] Although both CuO and Cu_2O photocathodes may undergo corrosion and experience degradation in photocurrent over time, the CuO photocathode appears to exhibit greater stability compared to Cu_2O.[167−170]

6. METAL NITRIDE-BASED PHOTOCATALYSTS AND THEIR IMPROVEMENT

6.1. Graphitic Carbon Nitride (g-C_3N_4). Graphitic carbon nitride (g-C_3N_4) possesses distinctive characteristics as a metal-free polymer and an n-type semiconductor, exhibiting exceptional attributes in terms of electrical, optical, structural, and physiochemical properties.[171] Generally, g-C_3N_4 has an optical wavelength of 460 nm and a band gap 2.7 eV, which means that it works with visible light.[172,173] Additionally, the other attributes of g-C_3N_4 include special facet properties, nonpoisonous character, abundance, and flexibility that lead to splitting of water with solar irradiation.[174,175] Bulk g-C_3N_4 has, however, a low photocatalytic efficiency because of disadvantages of high rates electron−hole pair recombination, the small g-C_3N_4 size (~10m^2/g), a tiny agile facet for connection, low surface response kinetics, insufficient visible absorption (less than 460 nm), mild oxidation, grain boundary implications, and poor charge mobility.[176] Various modifications have been implemented to limit these, including strategies like adjusting the band gap, employing micro- or nanoscale engineering, adopting bionic approaches, integrating cocatalysts, and enhancing surface properties.[177,178] The electrons produced in the presence of light are driven by a large thermodynamic driving power, suggesting that they have a high H_2 evolution potential in order to be capable of reducing various small molecules including H_2O, CO_2, and O_2. Attaining the correct electronic band alignment for g-C_3N_4 is crucial for its widespread application in the realm of photocatalytic water splitting. While the structure of g-C_3N_4 inherently supports a photocatalytic response, its performance in this regard is significantly hampered by the substantial challenges it faces. Substantial research on g-C_3N_4-based photocatalyst modifications for photocatalytic activities may improve the photocatalyst use of g-C_3N_4. The effectiveness of g-C_3N_4 can be enhanced through the introduction of metals and nonmetals and the creation of heterojunctions. The incorporation of dopant metals and nonmetals into active semiconductor photocatalysts is essential for modifying g-C_3N_4, as it can modify the band gap responsiveness to light and the reduction in band potential.[179,180]

N doping in g-C_3N_4 shows enhanced visible light absorption because of an impurity band forming in the vicinity of the valence band, and the synergistic effects of N doping facilitated the development and growing transfer of charges for enhanced hydrogen evolution.[181,182] Doping g-C_3N_4 with O reduced the optical band gap from 0.21 to 2.49 eV, which necessitates the consumption of complete photons by the natural sunlight. The doped material demonstrated approximately four times more photocatalytic activity as compared to pure g-C_3N_4 under identical circumstances. During the photocatalytic response, no evolution of nitrogen was detected, proving the stable H_2 production of O-doped g-C_3N_4. Utilizing metal doping serves as a viable approach for optimizing the band gap, as it substantially enhances light absorption, reduces the band gap, accelerates the movement of charges, and prolongs the lifespan of charge carriers. This results in an improved efficiency for photocatalytic processes. Pt doping to g-C_3N_4 contributes considerably to electrotrapping because of the Schottky barrier that allows efficient separation of charges. For an expanded region of the unique porous vacancy g-C_3N_4 with an enlarged surface region, the evolution of H_2 improved 13.5× as the capacity of the charge separation was enhanced. The adding of Pt as a cocatalyst enhanced photocatalytic activity because of the fact that the Schottky barrier was created to separate photogenerated electron−holes pairs. Pt and Co now have greater ability to boost photocatalytic operation in the codoping of g-C_3N_4.

Incorporating both metals and nonmetals into g-C_3N_4 can enhance the H_2 production, quantum yield, and sustainability. In summary, the combination of metal and nonmetal doping, along with the refinement of lone metal surfaces, when paired with organic dyes or quantum dots, has a notable impact on trapping and facilitating the transport of photogenerated electrons and holes across the semiconductor's surface under visible light irradiation. The use of nonmetals can alter the valence band position within the semiconductor's band gap, reducing the band gap energy and enabling greater involvement of visible light, while metals hold the promise of confining electrons through the Schottky barrier. As a result of the change in optical and electronic characteristics, doping g-C_3N_4 with metals and other nonmetals will increase the photocatalytic activity. Besides metallic and nonmetallic doping, the combination with semiconductors is also seen as an important approach for increasing the production of photocatalytic H_2. A photocatalyzer of water in hydrogen and oxygen, coupled with nanoparticles of RuO_2, is noted to be β-Ge_3N_4, a typical metallic nitride with a d^{10} electronic configuration.

7. METAL SULFIDE-BASED PHOTOCATALYSTS AND THEIR IMPROVEMENT

7.1. Zinc Sulfide (ZnS). ZnS nanostructures have been shown to provide strong photocatalysts, for example, halogenated benzene derivatives for photoreductive dehalogensis, CO_2 photoredox, photocatalysis, and photocatalytic water splitting to produce H_2. Moreover, ZnS has many advantages, including good transportation characteristics (reducing scattering and recombination of carriers), intrinsic n-type semiconductor properties, improved thermal stability, lofty electronic movement, nontoxic character, insolubility in water, and low cost. Photocatalysts with long wavelengths are highly desirable for efficient solar light collection. Indeed, a truly effective visible-light-initiated photocatalyst should not only operate efficiently under visible light but also demonstrate stability when exposed to sunlight irradiation. In developing visible-light-active photocatalysts that can use as much solar light as possible efficiently, many changes have been made. The synthesized of ZnS nanostructures include (a) bare ZnS nanoparticles of various morphology, including nanospheres, nanorods, nanotubes, and nanoflowers; (b) nanocomposites containing metal, nonmetal, and dye components with ZnS nanoparticles; and (c) ZnS nanostructures. ZnS is a quasi-conductive photocatalyst with a direct wide range with outstanding chemical stability against hydrolysis and oxidation if the size of the particles is only a meager few nanometers. However, due to a high charge, its photocatalytic efficiency is

https://doi.org/10.1021/acsomega.3c07822
ACS Omega 2024, 9, 6147−6164

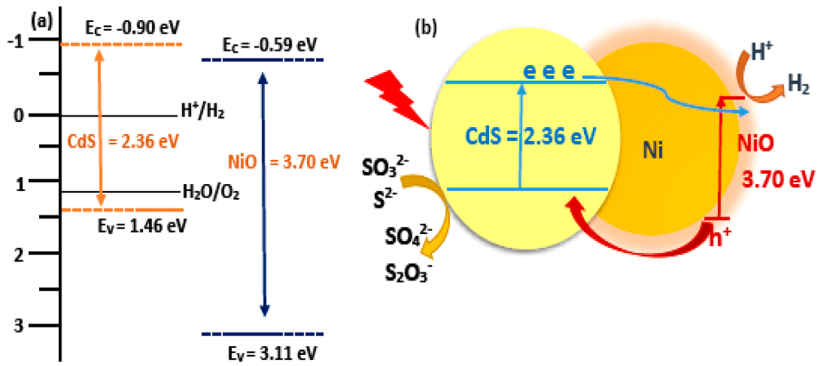

Figure 10. (a) Band position alignment and (b) charge transfer process for photocatalytic water splitting in the Ni@NiO-CdS heterostructure. Reprinted with permission from ref 183. Copyright 2021 Elsevier.

very low, and the rate of recovery and photocorrosion are not stable under irradiation. A conventional method of preparing efficient photocatalysts and light-responsive photocatalysts was loading a foreign substance into nonoxide ultraviolet-active photocatalysts. ZnS doped with noble metals has demonstrated its efficiency as a photocatalyst for the generation of hydrogen through water splitting under visible light irradiation.

7.2. Cadmium Sulfide (CdS). The energy band gap of cadmium sulfide is 2.4 eV, which is ideal for the solar spectrum. Owing to photocorrosion, CdS is not stable in aqueous solutions. Pure CdS's photocatalytic behavior is not that efficient. Many researchers focus primarily on the preparation of materials in which different morphologies and crystal CdS synthesis are used in order to address the problem; that is, a material change is used to enhance the photoactivity of the water splitting photocatalytic system. Recent research efforts have also been directed toward modifying CdS with metal sulfides such as MoS_2 and WS_2. This approach offers a promising avenue for enhancing the performance of CdS photocatalysis, providing a potential alternative to noble metal cocatalysts.

CdS electrons from the conduction band were moved to the Co facet, and the holes remained in the CdS valence band, resulting in efficient separation of charge. Moreover, the enhancement in hydrogen (H_2) evolution was attributed to its relatively low affinity for H^+ ions, which led to a reduction of H^+ ions to H_2 by the electrons present on the surface of cobalt (Co). In a separate experiment, composites consisting of CdS and NiSe nanorods exhibited improved photocatalytic performance and greater stability over a period of up to 30 hours. The Ni-loaded CdS nanorods was prepared and applied for the photocatalytic hydrogen (H_2) evolution under visible light irradiation. The Ni-loaded CdS photocatalysts delivered a synergic effect for photocatalytic water splitting H_2 evolution. The synergic effect was due to the formation of a NiO thin layer over the metallic Ni surface (Ni@NiO). The Ni@NiO in Ni@NiO-CdS acted as cocatalyst and trapped the photo-excited electrons from CdS for the reduction of protons (H^+) to produce H_2 at surface-interface between the Ni@NiO and CdS nanorods, resulting in the enhanced photoactivity for H_2 evolution.

8. CONCLUSION

This Review delves into the noteworthy advancements in photocatalysts for hydrogen (H_2) production, examining criteria for photocatalyst selection and various modifications to enhance the photocatalytic activity. The exploration encompasses diverse semiconductors, such as TiO_2, g-C_3N_4,[188] graphene, sulfides, oxides, nitrides, oxysulfides, oxynitrides, and cocatalyst-based photocatalysts. The discussion extends to techniques for improving the compatibility of metals and nonmetals to augment photoactivity under visible light irradiation.

A particular focus is placed on the development of heterojunctions, including type I, II, and III heterojunctions, as well as Z-scheme and S-scheme systems. Emphasis is placed on a comprehensive investigation of these aspects in the context of visible light radiation to enhance the efficacy of photocatalytic processes. Another notable advancement involves the incorporation of mediators, such as graphene oxide and metals, to establish indirect Z-scheme configurations with precise band adjustments. Consideration of reaction chemistry, mass transfer, kinetics, light diffusion limitations, and process intricacies and the selection of suitable light and photoreactors all contribute to optimizing sustainable hydrogen output efficiency and selectivity.

AUTHOR INFORMATION

Corresponding Authors

Dan Dobrotă − *Faculty of Engineering, Department of Industrial Engineering and Management, Lucian Blaga University of Sibiu, 550024 Sibiu, Romania;* orcid.org/0000-0002-2202-7701; Email: dan.dobrota@ulbsibiu.ro

Amit Kumar − *Centre for Augmented Intelligence and Design, Department of Mechanical Engineering, Sri Eshwar College of Engineering, Coimbatore, Tamil Nadu 641202, India;* Email: amit4310@rediffmail.com

Authors

Vikash Kumar − *Department of Electronics and Communication Engineering, RV Institute of Technology and Management, Bangalore, Karnataka 560076, India*

Gajendra Prasad Singh − *Department of Metallurgical and Material Engineering, Central University Jharkhand, Ranchi, Jharkhand 835205, India*

Manish Kumar − *Department of Mechanical Engineering, RV Institute of Technology and Management, Bangalore, Karnataka 560076, India*

Pooja Singh − *Department of Mechanical Engineering, Manipal University Jaipur, Jaipur, Rajasthan 303007, India*

Alok Kumar Ansu − *Department of Mechanical Engineering, Manipal University Jaipur, Jaipur, Rajasthan 303007, India*

Abhishek Sharma − *Department of Mechanical Engineering, BIT Sindri, Dhanbad, Jharkhand 828123, India*

https://doi.org/10.1021/acsomega.3c07822
ACS Omega 2024, 9, 6147−6164

Tabish Alam − *CSIR-Central Building Research Institute, Roorkee, Uttarakhand 247667, India*

Anil Singh Yadav − *Department of Mechanical Engineering, Bakhtiyarpur College of Engineering (Science, Technology and Technical Education Department, Government of Bihar), Bakhtiyarpur, Bihar 803212, India;* orcid.org/0000-0001-6786-2180

Complete contact information is available at: https://pubs.acs.org/10.1021/acsomega.3c07822

Notes

The authors declare no competing financial interest.

REFERENCES

(1) Hisatomi, T.; Domen, K. Introductory lecture: sunlight-driven water splitting and carbon dioxide reduction by heterogeneous semiconductor systems as key processes in artificial photosynthesis. *Faraday Discuss.* **2017**, *198*, 11−35.

(2) Wang, Q.; Hisatomi, T.; Jia, Q.; Tokudome, H.; Zhong, M.; Wang, C.; Pan, Z.; Takata, T.; Nakabayashi, M.; Shibata, N.; Li, Y.; Sharp, I. D.; Kudo, A.; Yamada, T.; Domen, K. Scalable water splitting on particulate photocatalyst sheets with a solar-to-hydrogen energy conversion e ciency exceeding 1%. *Nat. Mater.* **2016**, *15*, 611−15.

(3) Kibria, M. G.; Chowdhury, F. A.; Zhao, S.; AlOtaibi, B.; Trudeau, M. L.; Guo, H.; Mi, Z. Visible light-driven efficient overall water splitting using p-type metal-nitride nanowire arrays. *Nat. Commun.* **2015**, *6*, 6797.

(4) Pinaud, B. A.; Benck, J. D.; Seitz, L. C.; Forman, A. J.; Chen, Z.; Deutsch, T. G.; James, B. D.; Baum, K. N.; Baum, G. N.; Ardo, S.; Wang, H.; Miller, E.; Jaramillo, T. F. Technical and economic feasibility of centralized facilities for solar hydrogen production via photocatalysis and photoelectrochemistry. *Energy Environ. Sci.* **2013**, *6* (7), 1983−2002.

(5) Ager, J. W.; Shaner, M. R.; Walczak, K. A.; Sharp, I. D.; Ardo, S. Experimental demonstrations of spontaneous, solar-driven photoelectrochemical water splitting. *Energy Environ. Sci.* **2015**, *8* (10), 2811−24.

(6) Li, Z.; Luo, W.; Zhang, M.; Feng, J.; Zou, Z. Photoelectrochemical cells for solar hydrogen production: Current state of promising photoelectrodes, methods to improve their properties, and outlook. *Energy Environ. Sci.* **2013**, *6* (2), 347−70.

(7) Scheffe, J. R.; Li, J.; Weimer, A. W. A spinel ferrite/hercynite water-splitting redox cycle. *Int. J. Hydrogen Energy (Internet).* **2010**, *35* (8), 3333−40.

(8) Hisatomi, T.; Kubota, J.; Domen, K. Recent advances in semiconductors for photocatalytic and photoelectrochemical water splitting. *Chem. Soc. Rev.* **2014**, *43* (22), 7520−35.

(9) Ni, M.; Leung, M. K. H.; Leung, D. Y. C.; Sumathy, K. A review and recent developments in photocatalytic water-splitting using TiO2 for hydrogen production. *Renew Sustain Energy Rev.* **2007**, *11* (3), 401−25.

(10) Hu, X.; Li, Y.; Tian, J.; Yang, H.; Cui, H. Highly efficient full solar spectrum (UV-vis-NIR) photocatalytic performance of Ag2S quantum dot/TiO2 nanobelt heterostructures. *J. Ind. Eng. Chem. (Internet)* **2017**, *45*, 189−96.

(11) Sang, Y.; Liu, H.; Umar, A. Photocatalysis from UV/Vis to near-infrared light: Towards full solar-light spectrum activity. *ChemCatChem.* **2015**, *7* (4), 559−73.

(12) Tang, S.; Yin, X.; Wang, G.; Lu, X.; Lu, T. Single titanium-oxide species implanted in 2D g-C3N4 matrix as a highly efficient visible-light CO2 reduction photocatalyst. *Nano Res.* **2019**, *12* (2), 457−62.

(13) Sakar, M.; Nguyen, C. C.; Vu, M. H.; Do, T. O. Materials and Mechanisms of Photo-Assisted Chemical Reactions under Light and Dark Conditions: Can Day−Night Photocatalysis Be Achieved? *ChemSusChem.* **2018**, *11* (5), 809−20.

(14) Wafik, A. M.; Abd-El-Rahman, A. M.; Massoud, A. M.; Mazen, S. A. Composition dependence of discontinuous magnetization in $Cu_xFe_{3-x}O_{4+\delta}$. *J. Mat Sci.* **1997**, *32* (14), 3749−3752.

(15) Lan, Y.; Lu, Y.; Ren, Z. Mini review on photocatalysis of titanium dioxide nanoparticles and their solar applications. *Nano Energy (Internet)* **2013**, *2* (5), 1031−45.

(16) Fujishima, A.; Zhang, X.; Tryk, D. A. TiO2 photocatalysis and related surface phenomena. *Surf. Sci. Rep.* **2008**, *63* (12), 515−82.

(17) Hutter, E.; Fendler, J. H. Exploitation of localized surface plasmon resonance. *Adv. Mater.* **2004**, *16* (19), 1685−706.

(18) Petryayeva, E.; Krull, U. J. Localized surface plasmon resonance: Nanostructures, bioassays and biosensing-A review. *Anal Chim Acta (Internet).* **2011**, *706* (1), 8−24.

(19) Willets, K. A.; Van Duyne, R. P. Localized Surface Plasmon Resonance Spectroscopy and Sensing. *Annu. Rev. Phys. Chem.* **2007**, *58* (1), 267−97.

(20) Liu, J.; Wang, H.; Antonietti, M. Graphitic carbon nitride "reloaded": Emerging applications beyond (photo)catalysis. *Chem. Soc. Rev.* **2016**, *45* (8), 2308−26.

(21) Hasija, V.; Raizada, P.; Sudhaik, A.; Sharma, K.; Kumar, A.; Singh, P.; et al. Recent advances in noble metal free doped graphitic carbon nitride based nanohybrids for photocatalysis of organic contaminants in water: A review. *Appl. Mater. Today (Internet)* **2019**, *15*, 494−524.

(22) Callejas, J. F.; Read, C. G.; Roske, C. W.; Lewis, N. S.; Schaak, R. E. Synthesis, Characterization, and Properties of Metal Phosphide Catalysts for the Hydrogen-Evolution Reaction. *Chem. Mater.* **2016**, *28* (17), 6017−44.

(23) Shi, Y.; Zhang, B. Recent advances in transition metal phosphide nanomaterials: Synthesis and applications in hydrogen evolution reaction. *Chem. Soc. Rev. (Internet).* **2016**, *45* (6), 1529−41.

(24) Xue, W.; Huang, D.; Wen, X.; Chen, S.; Cheng, M.; Deng, R.; Li, B.; Yang, Y.; Liu, X. Silver-based semiconductor Z-scheme photocatalytic systems for environmental purification. *J. Hazard Mater.* **2020**, *390*, 122128.

(25) Nguyen, C. C.; Vu, N. N.; Do, T. O. Recent advances in the development of sunlight-driven hollow structure photocatalysts and their applications. *J. Mater. Chem. A* **2015**, *3* (36), 18345−59.

(26) Afroz, K.; Moniruddin, M.; Bakranov, N.; Kudaibergenov, S.; Nuraje, N. A heterojunction strategy to improve the visible light sensitive water splitting performance of photocatalytic materials. *J. Mater. Chem. A* **2018**, *6* (44), 21696−718.

(27) Shehzad, N.; Tahir, M.; Johari, K.; Murugesan, T.; Hussain, M. A critical review on TiO_2 based photocatalytic CO2 reduction system: Strategies to improve efficiency. *J. CO2 Util.* **2018**, *26*, 98−122.

(28) Yang, M. Q.; Gao, M.; Hong, M.; Ho, G. W. Visible-to-NIR Photon Harvesting: Progressive Engineering of Catalysts for Solar-Powered Environmental Purification and Fuel Production. *Adv. Mater.* **2018**, *30* (47), 1802894.

(29) Li, Z.; Ma, Y.; Hu, X.; Liu, E.; Fan, J. Enhanced photocatalytic H2 production over dual-cocatalyst-modified g-C3N4 heterojunctions. *Cuihua Xuebao/Chinese J. Catal. (Internet).* **2019**, *40* (3), 434−45.

(30) Liang, Z.; Dong, X.; Han, Y.; Geng, J. In-situ growth of 0D/2D Ni 2 P quantum dots/red phosphorus nanosheets with p-n heterojunction for efficient photocatalytic H 2 evolution under visible light. *Appl. Surf. Sci.* **2019**, *484*, 293−9.

(31) Li, Y.; Yin, Z.; Ji, G.; Liang, Z.; Xue, Y.; Guo, Y.; et al. 2D/2D/2D heterojunction of Ti3C2MXene/MoS2 nanosheets/TiO2 nanosheets with exposed (001) facets toward enhanced photocatalytic hydrogen production activity. *Appl. Catal. B Environ.* **2019**, *246*, 12−20.

(32) Moniz, S. J. A.; Shevlin, S. A.; Martin, D. J.; Guo, Z. X.; Tang, J. Visible-light driven heterojunction photocatalysts for water splitting-a critical review. *Energy Environ. Sci.* **2015**, *8* (3), 731−59.

(33) Ye, S.; Wang, R.; Wu, M. Z.; Yuan, Y. P. A review on g-C 3 N 4 for photocatalytic water splitting and CO 2 reduction. *Appl. Surf. Sci.* **2015**, *358*, 15−27.

(34) Li, X.; Shen, R.; Ma, S.; Chen, X.; Xie, J. Graphene-based heterojunction photocatalysts. *Appl. Surf. Sci.* **2018**, *430*, 53−107.
(35) Sébastien, S. Les soignants face à la mort. *Rev. Infirm.* **2012**, 39−41.
(36) Wu, N. L.; Lee, M. S. Enhanced TiO2 photocatalysis by Cu in hydrogen production from aqueous methanol solution. *Int. J. Hydrogen Energy.* **2004**, *29* (15), 1601−05.
(37) Ismail, A. A. Mesoporous PdO-TiO_2 nanocomposites with enhanced photocatalytic activity. *Appl. Catal. B Environ.* **2012**, *117*−*118*, 67−72.
(38) Park, H.; Park, Y.; Kim, W.; Choi, W. Surface modification of TiO2 photocatalyst for environmental applications. *J. Photochem. Photobiol. C Photochem. Rev.* **2013**, *15* (1), 1−20.
(39) Meshram, S. P.; Adhyapak, P. V.; Mulik, U. P.; Amalnerkar, D. P. Facile synthesis of CuO nanomorphs and their morphology dependent sunlight driven photocatalytic properties. *Chem. Eng. J.* **2012**, *204*−*206*, 158−68.
(40) Chang, Y.; Zeng, H. C. Manipulative Synthesis of Multipod Frameworks for Self-Organization and Self-Amplification of Cu_2O Microcrystals. *Cryst. Growth. Des.* **2004**, *4*, 273−278.
(41) Hsieh, C.-T.; Chen, J.-M.; Lin, H.-H.; Shih, H.-C. Field emission from various CuO nanostructures Field emission from various CuO nanostructures. *Appl. Phys. Lett.* **2003**, *83*, 3383−3385.
(42) Lanza, F.; Feduzi, R.; Fuger, J. Effects of lithium oxide on the electrical properties of CuO at low temperatures. *J. Mater. Res.* **1990**, *5*, 1739−1744.
(43) Li, G.; Dimitrijevic, N. M.; Chen, L.; Rajh, T.; Gray, K. A. Role of Surface/Interfacial Cu 2 + Sites in the Photocatalytic Activity of Coupled CuO - TiO 2 Nanocomposites. *J. PHys. Chem. C.* **2008**, *112*, 19040−19044.
(44) Zhang, X.; Jin, Z.; Li, Y.; Li, S.; Lu, G. *Visible-light-induced hydrogen production over Pt-Eosin Y catalysts with high surface area silica gel as matrix* **2007**, *166*, 74−9.
(45) Xu, Y.; Gao, S. Band gap of C 3 N 4 in the GW approximation. *Int. J. Hydrogen Energy.* **2012**, *37* (15), 11072−80.
(46) Liu, J.; Zhang, T.; Wang, Z.; Dawson, G.; Chen, W. Simple pyrolysis of urea into graphitic carbon nitride with recyclable adsorption and photocatalytic activity. *J. Mater. Chem.* **2011**, *21* (38), 14398−401.
(47) Maeda, K.; Wang, X.; Nishihara, Y.; Lu, D.; Antonietti, M.; Domen, K. *Photocatalytic Activities of Graphitic Carbon Nitride Powder for Water Reduction and Oxidation under Visible Light.* **2009**, *113*, 4940−7.
(48) Suryawanshi, A.; Dhanasekaran, P.; Mhamane, D.; Kelkar, S.; Patil, S.; Gupta, N.; Ogale, S. Doubling of photocatalytic H 2 evolution from g-C 3 N 4 via its nanocomposite formation with multiwall carbon nanotubes : Electronic and morphological effects. *Int. J. Hydrogen Energy.* **2012**, *37* (12), 9584−9589.
(49) Li, S.; Zhang, L.; Jiang, T.; Chen, L.; Lin, Y.; Wang, D.; Xie, T. Construction of Shallow Surface States through Light Ni Doping for High-Efficiency Photocatalytic Hydrogen Production of CdS Nanocrystals. *Chem. Eur. J.* **2014**, *20* (1), 311−316.
(50) Fu, C. F.; Luo, Q.; Li, X.; Yang, J. Two-dimensional van der Waals nanocomposites as Z-scheme type photocatalysts for hydrogen production from overall water splitting. *J. Materials Chemistry A* **2016**, *4* (48), 18892−98.
(51) Cao, S.; Li, H.; Li, Y.; Zhu, B.; Yu, J. Dependence of exposed facet of Pd on photocatalytic H2-production activity. *ACS Sustainable Chem. Eng.* **2018**, *6* (5), 6478−6487.
(52) Ismail, A. A.; Ibrahim, I. A. Impact of supercritical drying and heat treatment on physical properties of titania/silica aerogel monolithic and its applications. *Appl. Catal. A* **2008**, *346*, 200−205.
(53) Ran, J.; Gao, G.; Li, F.; Ma, T.; Du, A.; Qiao, S. Ti3C2 MXene co-catalyst on metal sulfide photo-absorbers for enhanced visible-light photocatalytic photocatalytic hydrogen production. *Nat. Commun.* **2017**, *8*, 13907.
(54) Reddy, D. A.; Kim, E. H.; Gopannagari, M.; Ma, R.; Bhavani, P.; Kumar, D. P. Enhanced Photocatalytic Hydrogen Evolution by Integrating Dual Co-Catalysts on Heterophase CdS Nano-Junctions. *ACS Sustainable Chem. Eng.* **2018**, *6* (10), 12835−12844.
(55) Zhong, X.; Tang, J.; Wang, J.; Shao, M.; Chai, J.; Wang, S. AC SC. *Electrochim. Acta* **2018**, *269*, 55.
(56) Ismail, A. A.; Robben, L.; Bahnemann, D. W. Study of the Efficiency of UV and Visible-Light Photocatalytic Oxidation of Methanol on Mesoporous RuO_2-TiO_2Nanocomposites. *ChemPhysChem* **2011**, *12*, 982−91.
(57) Wang, X.; Maeda, K.; Thomas, A.; Takanabe, K.; Xin, G.; Carlsson, J. M.; et al. A metal-free polymeric photocatalyst for hydrogen production from water under visible light. *Nat. Mater. (Internet).* **2009**, *8* (1), 76−80.
(58) Nguyen, M.; Tran, P. D.; Pramana, S. S.; Lee, R. L.; Batabyal, S. K.; Mathews, N.; Wong, L. H.; Graetzel, M. In situ photo-assisted deposition of MoS2 electrocatalyst onto zinc cadmium sulphide nanoparticle surfaces to construct an efficient photocatalyst for hydrogen generation. *Nanoscale* **2013**, *5* (4), 1479−82.
(59) Osterloh, F. E. Inorganic Materials as Catalysts for Photochemical Splitting of Water. *Chem. Mater.* **2008**, *20*, 35−54.
(60) Chang, K.; Hai, X.; Pang, H.; Zhang, H.; Shi, L.; Liu, G.; Liu, H.; Zhao, G.; Li, M.; Ye, J.; et al. Targeted Synthesis of 2H- and 1T-Phase MoS 2 Monolayers for Catalytic Hydrogen Evolution. *Adv. Mater.* **2016**, *28*, 10033−10041.
(61) Yi, S.-S.; Yan, J.-M.; Wulan, B.-R.; Li, S.-J.; Liu, K.-H.; Jiang, Q. Noble-Metal-Free Cobalt Phosphide Modified Carbon Nitride : an Efficient Photocatalyst for Hydrogen Generation. *Appl. Catal. B* **2017**, *200*, 477−483.
(62) Linsebigler, A. L.; Lu, G.; Yates, J. T. Photocatalysis on TiO2 Surfaces: Principles, Mechanisms, and Selected Results. *Chem. Rev.* **1995**, *95* (3), 735−58.
(63) Kong, C.; Min, S.; Lu, G. Robust Pt−Sn alloy decorated graphene nanohybrid cocatalyst for photocatalytic hydrogen evolution. *Chem. Commu.* **2014**, *50* (66), 9281−9283.
(64) Xie, X.; Zhang, N.; Tang, Z.; Anpo, M.; Xu, Y. Ti3C2Tx MXene as a Janus cocatalyst for concurrent promoted photoactivity and inhibited photocorrosion. *Appl. Catal. B* **2018**, *237*, 43−49.
(65) Shehzad, N.; Tahir, M.; Johari, K.; Murugesan, T.; Hussain, M. Fabrication of highly efficient and stable indirect Z-scheme assembly of AgBr/TiO2 via graphene as a solid-state electron mediator for visible light induced enhanced photocatalytic H2 production. *Appl. Surf. Sci.* **2019**, *463*, 445−55.
(66) Kandiel, T. A.; Ismail, A.; Bahnemann, D. W. Mesoporous TiO 2 nanostructures : a route to minimize Pt loading on titania photocatalysts for hydrogen production. *Phys. Chem. Chem. Phys.* **2011**, *13*, 20155.
(67) Ismail, A. A.; Bahnemann, D. W. Solar Energy Materials & Solar Cells Photochemical splitting of water for hydrogen production by photocatalysis : A review. *Sol Energy Mater. Sol Cells* **2014**, *128*, 85−101.
(68) Ismail, A. A.; Bahnemann, D. W. *Mesostructured Pt/TiO 2 Nanocomposites as Highly Active Photocatalysts for the Photooxidation of Dichloroacetic Acid* **2011**, *115*, 5784−91.
(69) Tong, H.; Ouyang, S.; Bi, Y.; Umezawa, N.; Oshikiri, M.; Ye, J. Nano-photocatalytic Materials : Possibilities and Challenges. *Adv. Mater.* **2012**, *24*, 229−251.
(70) Wen, J.; Xie, J.; Chen, X.; Li, X. Applied Surface Science A review on g-C 3 N 4 -based photocatalysts. *Appl. Surf. Sci. (Internet).* **2017**, *391*, 72−123.
(71) Yang, Z.; Chu, D.; Jia, G.; Yao, M.; Liu, B. Significantly narrowed bandgap and enhanced charge separation in porous, nitrogen-vacancy red g-C3 N4 for visible light photocatalytic H2 production. *Appl. Surf. Sci.* **2020**, *504*, No. 144407.
(72) Chiarello, G. L.; Aguirre, M. H.; Selli, E. Hydrogen production by photocatalytic steam reforming of methanol on noble. *J. Catal.* **2010**, *273* (2), 182−190.
(73) Tahir, M.; Amin, N. S. Advances in visible light responsive titanium oxide-based photocatalysts for CO 2 conversion to hydrocarbon fuels. *Energy Convers Manag.* **2013**, *76*, 194−214.

https://doi.org/10.1021/acsomega.3c07822
ACS Omega 2024, 9, 6147−6164

(74) Huang, J.; Li, L.; Chen, J.; Ma, F.; Yu, Y. ScienceDirect Broad spectrum response flower spherical-like composites CQDs@ CdIn2S4/CdS modified by CQDs with up-conversion property for photocatalytic degradation and water splitting. *Int. J. Hydrogen Energy.* **2020**, *45* (3), 1822−36.
(75) Tahir, M.; Tasleem, S.; Tahir, B. Recent development in band engineering of binary semiconductor materials for solar driven photocatalytic hydrogen production. *Int. J. Hydrogen Energy.* **2020**, *45* (32), 15985−16038.
(76) Yue, X.; Hou, J.; Zhao, H.; Wu, P.; Guo, Y.; Shi, Q.; et al. Au-Ag alloy nanoparticles with tunable cavity for plasmon-enhanced photocatalytic H2 evolution. *J. Energy Chem.* **2020**, *49*, 1−7.
(77) Jang, J. S.; Kim, H. G.; Lee, J. S. Heterojunction semiconductors : A strategy to develop efficient photocatalytic materials for visible light water splitting. *Catal. Today.* **2012**, *185* (1), 270−277.
(78) Low, J.; Yu, J.; Jaroniec, M.; Wageh, S.; Al-ghamdi, A. A. Heterojunction Photocatalysts. *Adv. Mater.* **2017**, *29* (20), 1601694.
(79) Nasir, S. N. F. M.; Ullah, H.; Ebadi, M.; Tahir, A. A.; Sagu, J. S.; Mat Teridi, M. A.; et al. New Insights into Se/BiVO Heterostructure for Photoelectrochemical Water Splitting : A Combined Experimental and DFT Study. *J. Phy Chem.* **2017**, *121* (11), 6218−28.
(80) Zhu, Y.; Wan, T.; Wen, X.; Chu, D.; Jiang, Y. Tunable Type I and II heterojunction of CoOx nanoparticles confined in g-C3N4 nanotubes for photocatalytic hydrogen production. *Applied Catal. B, Environ.* **2019**, *244*, 814−22.
(81) Xu, F.; Zhang, L.; Cheng, B.; Yu, J. Direct Z-scheme TiO2/NiS core-shell hybrid nanofibers with enhanced photocatalytic H2-production activity. *ACS Sustainable Chem. & Eng.* **2018**, *6* (9), 12291−98.
(82) Xu, Q.; Zhang, L.; Yu, J.; Wageh, S.; Al-ghamdi, A. A.; Jaroniec, M. Direct Z-scheme photocatalysts : Principles, synthesis, and applications. *Mater. Today* **2018**, *21* (10), 1042−63.
(83) Maeda, K. Z-scheme Water Splitting using Two Different Semiconductor Photocatalysts. *ACS Catal.* **2013**, *3* (7), 1486−1503.
(84) Kumar, N.; Karmakar, S.; Kumar, D.; Kumar, A.; Bishnoi, P. Energy, economics and environmental (3E's) analysis of a solar-assisted HRES through demand side management. *Environ. Sci. Pollut. Res.* **2023**, DOI: 10.1007/s11356-023-29329-4.
(85) Tahir, M.; Siraj, M.; Tahir, B.; Umer, M.; Alias, H.; Othman, N. Au-NPs embedded Z − scheme WO3/TiO2 nanocomposite for plasmon-assisted photocatalytic glycerol-water reforming towards enhanced H 2 evolution. *Appl. Surf. Sci.* **2020**, *503*, No. 144344.
(86) Singh, P.; Ansu, A. K.; Sharma, R. K.; Kumari, P.; Kumar, A.; Kumar, R. Development, Thermal Properties, and Reliability Testing of Eutectic Polyethylene Glycol as Phase Change Materials for Thermal Energy Storage Applications. *Int. J. Thermophys.* **2023**, *44* (3), 39.
(87) Kumar, A.; Layek, A.; Mondal, P. K. Heat Transfer Analysis of a Solar Air Heater Roughened with Chamfered Rib and Groove Roughness on the Absorber Plate Using CFD Approach. In *Advances in Mechanical Engineering*; Biswal, B. B., Sarkar, B. K., Mahanta, P., Eds.; Springer, 2020; pp 1373−1384.
(88) Umer, M.; Tahir, M.; Azam, M. U.; Jaffar, M. M. Metal free MWCNTs@TiO2@MMT heterojunction composite with MMT as a mediator for fast charges separation towards visible light driven photocatalytic hydrogen evolution. *Appl. Surf. Sci.* **2019**, *463*, 747−757.
(89) Kumar, D.; Kumar, A.; Kumar, N.; Sharma, A.; Choudhury, R.; Faisal, N.; Singh, R. K.; Mane, B. K. Current Trends, Regulations, Challenges, and Management Strategies of E-Waste in India. In *Sustainable Approaches and Strategies for E-Waste Management and Utilization*; IGI Global: Hershey, PA, 2023; pp 1−25).
(90) Azam, M. U.; Tahir, M.; Umer, M.; Jaffar, M. M.; Nawawi, M.G.M. Applied Surface Science Engineering approach to enhance photocatalytic water splitting for dynamic H2 production using La2O3/TiO2 nanocatalyst in a monolith photoreactor. *App Surf. Sci.* **2019**, *484*, 1089−1101.
(91) Chen, W.; Liu, M.; Wang, Y.; Gao, L.; Dang, H.; Mao, L. Non-noble metal Co as active sites on TiO 2 nanorod for promoting photocatalytic H2 production. *Mater. Res. Bull.* **2019**, *116*, 16−21.
(92) Tian, H.; Kang, S. Z.; Li, X.; Qin, L.; Ji, M.; Mu, J. Fabrication of an efficient noble metal-free TiO2-based photocatalytic system using Cu-Ni bimetallic deposit as an active center of H2 evolution from water. *Sol Energy Mater. Sol Cells.* **2015**, *134*, 309−17.
(93) Tanigawa, S.; Irie, H. Visible-light-sensitive two-step overall water-splitting based on band structure control of titanium dioxide. *Appl. Catal. B Environ.* **2016**, *180*, 1−5.
(94) Shen, J.; Meng, Y.; Xin, G. CdS/TiO 2 nanotubes hybrid as visible light driven photocatalyst for water splitting. *Rare Met.* **2011**, *30* (SUPPL.1), 280−283.
(95) Mokhtar, S. B.; Kait, C. F. Photohydrogen production from sea water using Fe/TiO2. *AIP Conf Proc.* **2012**, *1482*, 525−529.
(96) Le, T. T.; Akhtar, M. S.; Park, D. M.; Lee, J. C.; Yang, O. B. Water splitting on Rhodamine-B dye sensitized Co-doped TiO 2 catalyst under visible light. *Appl. Catal. B Environ.* **2012**, *111−112*, 397−401.
(97) Lalitha, K.; Reddy, J. K.; Phanikrishna Sharma, M. V.; Kumari, V. D.; Subrahmanyam, M. Continuous hydrogen production activity over finely dispersed Ag2O/TiO2 catalysts from methanol:water mixtures under solar irradiation: A structure-activity correlation. *Int. J. Hydrogen Energy.* **2010**, *35* (9), 3991−4001.
(98) Babu, V. J.; Kumar, M. K.; Nair, A. S.; Kheng, T. L.; Allakhverdiev, S. I.; Ramakrishna, S. Visible light photocatalytic water splitting for hydrogen production from N-TiO 2 rice grain shaped electrospun nanostructures. *Int. J. Hydrogen Energy.* **2012**, *37* (10), 8897−904.
(99) Nada, A. A.; Hamed, H. A.; Barakat, M. H.; Mohamed, N. R.; Veziroglu, T. N. Enhancement of photocatalytic hydrogen production rate using photosensitized TiO2/RuO2-MV2+. *Int. J. Hydrogen Energy.* **2008**, *33* (13), 3264−9.
(100) Strataki, N.; Bekiari, V.; Kondarides, D. I.; Lianos, P. Hydrogen production by photocatalytic alcohol reforming employing highly efficient nanocrystalline titania films. *Appl. Catal. B Environ.* **2007**, *77* (1−2), 184−9.
(101) Wang, Q.; An, N.; Bai, Y.; Hang, H.; Li, J.; Lu, X.; et al. High photocatalytic hydrogen production from methanol aqueous solution using the photocatalysts CuS/TiO2. *Int. J. Hydrogen Energy.* **2013**, *38* (25), 10739−45.
(102) Agegnehu, A. K.; Pan, C. J.; Tsai, M. C.; Rick, J.; Su, W. N.; Lee, J. F.; et al. Visible light responsive noble metal-free nano-composite of V-doped TiO2 nanorod with highly reduced graphene oxide for enhanced solar H2 production. *Int. J. Hydrogen Energy.* **2016**, *41* (16), 6752−62.
(103) Gao, D.; Wu, X.; Wang, P.; Xu, Y.; Yu, H.; Yu, J. Simultaneous Realization of Direct Photoinduced Deposition and Improved H2-Evolution Performance of Sn-Nanoparticle-Modified TiO2 Photo-catalyst. ACS Sustain. *Chem. Eng.* **2019**, *7*, 10084−10094.
(104) Udayabhanu; Lakshmana Reddy, N.; Shankar, M.V.; Sharma, S.C.; Nagaraju, G. One-pot synthesis of CueTiO2/CuO nano-composite : Application to photocatalysis for enhanced H2 production, dye degradation & detoxification of Cr,. *Int. J. Hydrogen Energy.* **2020**, *45* (13), 7813−7828.
(105) Piskunov, S.; Lisovski, O.; Begens, J.; Bocharov, D.; Zhukovskii, Y. F.; Wessel, M.; Spohr, E. C- N- S- and Fe- doped TiO2 Nanotubes for Visible-Light-Driven Photocatalytic Water Splitting : Prediction from First Principles. *J. Phy Chem.* **2015**, *119* (32), 18686−18696.
(106) Luo, H.; Takata, T.; Lee, Y.; Zhao, J.; Domen, K.; Yan, Y. Photocatalytic Activity Enhancing for Titanium Dioxide by Co-doping with Bromine and Chlorine. *Chem. Mater.* **2004**, *16*, 846−849.
(107) Wu, J. C.; Chen, C. A visible-light response vanadium-doped titania nanocatalyst by sol-gel method. *J. Photochem. and Photobio.* **2004**, *163* (1), 509−15.
(108) Nguyen, C.-C.; Nguyen, D. T.; Do, T.-O. A novel route to synthesize C/Pt/TiO2 phase tunable anatase−Rutile TiO2 for

https://doi.org/10.1021/acsomega.3c07822
ACS Omega 2024, 9, 6147−6164

efficient sunlight-driven photocatalytic applications. *Applied Catal. B* **2018**, *226*, 46−52.
(109) Wang, D.; Pillai, S. C.; Ho, S.; Zeng, J.; Li, Y.; Dionysiou, D. D. Plasmonic-based nanomaterials for environmental remediation. *Appl. Catal. B* **2018**, *237*, 721−741.
(110) Liu, E.; Kang, L.; Yang, Y.; Sun, T.; Hu, X.; Zhu, C.; Liu, H.; Wang, Q.; Li, X.; Fan, J. Plasmonic Ag deposited TiO 2 nano-sheet film for enhanced photocatalytic hydrogen production by water splitting. *Nanotechnology* **2014**, *25* (16), No. 165401.
(111) Linic, S.; Christopher, P.; Ingram, D. B. Plasmonic-metal nanostructures for efficient conversion of solar to chemical energy. *Nat. Publ Gr.* **2011**, *10* (12), 911−21.
(112) Tahir, M. Ni/MMT-promoted TiO2 nanocatalyst for dynamic photocatalytic H2 and hydrocarbons production from ethanol-water mixture under UV-light. *Int. J. Hydrogen Energy.* **2017**, *42* (47), 28309−26.
(113) Gallegos, M. V.; Peluso, M. A.; Thomas, H.; Damonte, L. C.; Sambeth, J. E. Structural and optical properties of ZnO and manganese-doped ZnO. *J. Alloys Compd (Internet)* **2016**, *689*, 416−24.
(114) Özgur, Ü.; Alivov, Y. I.; Liu, C.; Teke, A.; Reshchikov, M. A.; Doğan, S.; Avrutin, V.; Cho, S.-J.; Morkoç, H.; et al. A comprehensive review of ZnO materials and devices. *J. Appl. Phys.* **2005**, *98* (4), 041301.
(115) Bai, Y.; Yu, H.; Li, Z.; Amal, R.; Lu, G. Q.; Wang, L. In situ growth of a ZnO nanowire network within a TiO2 nanoparticle film for enhanced dye-sensitized solar cell performance. *Adv. Mater.* **2012**, *24* (43), 5850−6.
(116) Han, Z.; Liao, L.; Wu, Y.; Pan, H.; Shen, S.; Chen, J. Synthesis and photocatalytic application of oriented hierarchical ZnO flower-rod architectures. *J. Hazard Mater.* **2012**, *217*−*218*, 100−6.
(117) Kumaran, N. N.; Muraleedharan, K. Photocatalytic activity of ZnO and Sr2+ doped ZnO nanoparticles. *J. Water Process Eng.* **2017**, *17*, 264−70.
(118) Zhang, H.; Liu, F.; Mou, Z.; Liu, X.; Sun, J.; Lei, W. A facile one-step synthesis of ZnO quantum dots modified poly(triazine imide) nanosheets for enhanced hydrogen evolution under visible light. *Chem. Commun.* **2016**, *52* (88), 13020−3.
(119) Kalinauskas, P.; Valsiūnas, I.; Samulevičien, M.; Juzeliūnas, E. Zinc photo-corrosion in neutral solutions. *Corros. Sci.* **2001**, *43* (11), 2083−2092.
(120) Doménech, J.; Prieto, A. Stability of ZnO particles in aqueous suspensions under UV illumination. *J. Phys. Chem.* **1986**, *90* (6), 1123−6.
(121) Lee, K. M.; Lai, C. W.; Ngai, K. S.; Juan, J. C. Recent developments of zinc oxide based photocatalyst in water treatment technology: A review. *Water Res.* **2016**, *88*, 428−48.
(122) Kang, K.; Jimeng, X.; Xitao, W. The effects of ZnO morphology on photocatalytic efficiency of ZnO/RGO nano-composites. *Appl. Surf. Sci.* **2016**, *360*, 270−275.
(123) Chang, X.; Li, Z.; Zhai, X.; Sun, S.; Gu, D.; Dong, L.; Yin, Y.; Zhu, Y. Efficient synthesis of sunlight-driven ZnO-based heterogeneous photocatalysts. *Mater. Des.* **2016**, *98*, 324−332.
(124) Wang, H.; Zhang, L.; Chen, Z.; Hu, J.; Li, S.; Wang, Z.; Liu, J.; Wang, X. Semiconductor heterojunction photocatalysts: Design, construction, and photocatalytic performances. *Chem. Soc. Rev.* **2014**, *43*, 5234−5244.
(125) Carabineiro, S. A. C.; MacHado, B. F.; Bacsa, R. R.; Serp, P.; Dražić, G.; Faria, J. L.; Figueiredo, J. L.; et al. Catalytic performance of Au/ZnO nanocatalysts for CO oxidation. *J. Catal.* **2010**, *273* (2), 191−198.
(126) Primo, A.; Corma, A.; García, H. Titania supported gold nanoparticles as photocatalyst. *Phys. Chem. Chem. Phys.* **2011**, *13* (3), 886−910.
(127) Carneiro, J. T.; Savenije, T. J.; Moulijn, J. A.; Mul, G. The effect of Au on TiO2 catalyzed selective photocatalytic oxidation of cyclohexane. *J. Photochem. Photobiol. A Chem.* **2011**, *217* (2−3), 326−32.
(128) Silva, C. G.; Sampaio, M. J.; Carabineiro, S. A. C.; Oliveira, J. W. L.; Baptista, D. L.; Bacsa, R.; et al. Developing highly active photocatalysts: Gold-loaded ZnO for solar phenol oxidation. *J. Catal.* **2014**, *316*, 182−90.
(129) Silva, A. M. T.; Zilhão, N. R.; Segundo, R. A.; Azenha, M.; Fidalgo, F.; Silva, A. F.; et al. Photo-Fenton plus Solanum nigrum L. weed plants integrated process for the abatement of highly concentrated metalaxyl on waste waters. *Chem. Eng. J.* **2012**, *184*, 213−20.
(130) Landmann, M.; Rauls, E.; Schmidt, W. G. The electronic structure and optical response of rutile, anatase and brookite TiO 2. *J. Phys.: Condens. Matter* **2012**, *24* (19), 195503.
(131) Yoo, H.; Kahng, S.; Hyeun Kim, J. Z-scheme assisted ZnO/Cu2O-CuO photocatalysts to increase photoactive electrons in hydrogen evolution by water splitting. *Sol Energy Mater. Sol Cells.* **2020**, *204*, No. 110211.
(132) Kanade, K. G.; Kale, B. B.; Baeg, J.; Lee, S. M.; Lee, C. W.; Moon, S. J.; Chang, H. Self-assembled aligned Cu doped ZnO nanoparticles for photocatalytic hydrogen production under visible light irradiation. *Mater. Chem. Phys.* **2007**, *102* (1), 98−104.
(133) Xie, M. Y.; Su, K. Y.; Peng, X. Y.; Wu, R. J.; Chavali, M.; Chang, W. C. Hydrogen production by photocatalytic water-splitting on Pt-doped TiO2−ZnO under visible light. *J. Taiwan Inst. Chem. Eng.* **2017**, *70*, 161−167.
(134) Haldorai, Y.; Shim, J. J. Supercritical fluid mediated synthesis of highly exfoliated graphene/ZnO composite for photocatalytic hydrogen production. *Mater. Lett.* **2014**, *133* (3), 24−27.
(135) Zhang, Y. H.; et al. Facile synthesis of core−shell Cu2O@ZnO structure with enhanced photocatalytic H2 production. *J. Phys. Chem. Solids.* **2018**, *116*, 126−130.
(136) Wang, X.; Liu, G.; Lu, G. Q.; Cheng, H. M. Stable photocatalytic hydrogen evolution from water over ZnO-CdS core-shell nanorods. *Int. J. Hydrogen Energy* **2010**, *35* (15), 8199−8205.
(137) Zhao, J.; Zhang, P.; Fan, J.; Hu, J.; Shao, G. Constructing 2D layered MoS 2 nanosheets-modified Z-scheme TiO 2 /WO 3 nanofibers ternary nanojunction with enhanced photocatalytic activity. *Appl. Surf. Sci.* **2018**, *430*, 466−74.
(138) Katsumata, H.; Tachi, Y.; Suzuki, T.; Kaneco, S. Z-scheme photocatalytic hydrogen production over WO3/g-C 3N4 composite photocatalysts. *RSC Adv.* **2014**, *4* (41), 21405−9.
(139) Hu, T.; Li, P.; Zhang, J.; Liang, C.; Dai, K. Highly efficient direct Z-scheme WO 3 /CdS-diethylenetriamine photocatalyst and its enhanced photocatalytic H2 evolution under visible light irradiation. *Appl. Surf. Sci.* **2018**, *442*, 20−9.
(140) Toledo Camacho, S. Y.; Rey, A.; Hernández-Alonso, M. D.; Llorca, J.; Medina, F.; Contreras, S. Pd/TiO 2 -WO 3 photocatalysts for hydrogen generation from water-methanol mixtures. *Appl. Surf. Sci.* **2018**, *455*, 570−80.
(141) Wang, H.; Li, C.; Ying, L.; Fang, P. WO 3 &WS 2 nanorods coupled with CdS nanoparticles for enhanced visible light driven hydrogen evolution. *Appl. Surf. Sci. (Internet)* **2018**, *448*, 539−46.
(142) Zhang, L. J.; et al. Highly Efficient CdS/WO 3 Photocatalysts : Z- Scheme Photocatalytic Mechanism for Their Enhanced Photocatalytic H 2 Evolution under Visible light. *ACS Catal.* **2014**, *4* (10), 3724−29.
(143) Riboni, F.; Bettini, L. G.; Bahnemann, D. W.; Selli, E. WO3-TiO2 vs. TiO2 photocatalysts: Effect of the W precursor and amount on the photocatalytic activity of mixed oxides. *Catal. Today.* **2013**, *209*, 28−34.
(144) Spanu, D.; Recchia, S.; Mohajernia, S.; Schmuki, P.; Altomare, M. Site-selective Pt dewetting on WO3-coated TiO2 nanotube arrays: An electron transfer cascade-based H2 evolution photocatalyst. *Appl. Catal. B Environ.* **2018**, *237*, 198−205.
(145) Tanaka, A.; Hashimoto, K.; Kominami, H. Visible-light-induced hydrogen and oxygen formation over Pt/Au/WO 3 photocatalyst utilizing two types of photoabsorption due to surface plasmon resonance and band-gap excitation. *J. Am. Chem. Soc.* **2014**, *136* (2), 586−9.

https://doi.org/10.1021/acsomega.3c07822
ACS Omega 2024, 9, 6147−6164

(146) Sivula, K.; Formal, F Le; Grätzel, M. WO3-Fe2O3 photoanodes for water splitting: A host scaffold, guest absorber approach. *Chem. Mater.* **2009**, *21* (13), 2862−7.
(147) Hung, W. H.; Chien, T. M.; Tseng, C. M. Enhanced photocatalytic water splitting by plasmonic TiO 2-Fe2O3 cocatalyst under visible light irradiation. *J. Phys. Chem. C* **2014**, *118* (24), 12676−81.
(148) Thimsen, E.; Le Formal, F.; Grätzel, M.; Warren, S. C. Influence of plasmonic Au nanoparticles on the photoactivity of Fe 2O3 electrodes for water splitting. *Nano Lett.* **2011**, *11* (1), 35−43.
(149) Ling, Y.; Wang, G.; Wheeler, D. A.; Zhang, J. Z.; Li, Y. Sn-doped hematite nanostructures for photoelectrochemical water splitting. *Nano Lett.* **2011**, *11* (5), 2119−25.
(150) Kleiman-Shwarsctein, A.; Hu, Y. S.; Forman, A. J.; Stucky, G. D.; McFarland, E. W. Electrodeposition of α-Fe2O3 doped with Mo or Cr as photoanodes for photocatalytic water splitting. *J. Phys. Chem. C* **2008**, *112* (40), 15900−7.
(151) Hu, Y.; Kleiman-shwarsctein, A.; Forman, A. J.; Hazen, D.; Park, J.; Mcfarland, E. W.; et al. Pt-Doped r -Fe 2 O 3 Thin Films Active for Photoelectrochemical Water Splitting. *Chem. Mater.* **2008**, *20* (12), 3803−5.
(152) Liu, X.; Jin, A.; Jia, Y.; Jiang, J.; Hu, N.; Chen, X. Facile synthesis and enhanced visible-light photocatalytic activity of graphitic carbon nitride decorated with ultrafine Fe2O3 nanoparticles. *RSC Adv.* **2015**, *5* (112), 92033−41.
(153) Zhu, S.; et al. Fe2O3/TiO2 photocatalyst of hierarchical structure for H2 production from water under visible light irradiation. *Microporous Mesoporous Mater.* **2014**, *190*, 10−16.
(154) Imran, M.; Yousaf, A B.; Kasak, P.; Zeb, A.; Zaidi, S. J. Highly efficient sustainable photocatalytic Z-scheme hydrogen production from an A-Fe2O3 engineered ZnCdS heterostructure. *J. Catal.* **2017**, *353*, 81−88.
(155) Shen, H.; Liu, G.; Yan, X.; Jiang, J.; Hong, Y.; Yan, M.; et al. All-solid-state Z-scheme system of RGO-Cu2O/Fe2O3 for simultaneous hydrogen production and tetracycline degradation. *Mater. Today Energy.* **2017**, *5*, 312−9.
(156) Li, Y.-p.; Li, F.-t.; Wang, X.-j.; Zhao, J.; Wei, J.-n.; Hao, Y.-j.; Liu, Y.; et al. Z-scheme electronic transfer of quantum-sized A-Fe2O3 modified g-C3N4 hybrids for enhanced photocatalytic hydrogen production. *Int. J. Hydrogen Energy.* **2017**, *42* (47), 28327−28336.
(157) Long, M.-c.; Beranek, R.; Cai, W.-m.; Kisch, H. Hybrid semiconductor electrodes for light-driven photoelectrochemical switches. *Electrochim. Acta* **2008**, *53* (14), 4621−4626.
(158) Paracchino, A.; Laporte, V.; Sivula, K.; Grätzel, M.; Thimsen, E. Highly active oxide photocathode for photoelectrochemical water reduction. *Nat. Mater.* **2011**, *10* (6), 456−61.
(159) Barreca, D.; Fornasiero, P.; Gasparotto, A.; Gombac, V.; Maccato, C.; Montini, T.; et al. The potential of supported Cu2O and CuO nanosystems in photocatalytic H2 production. *ChemSusChem.* **2009**, *2* (3), 230−3.
(160) Chaudhary, Y. S.; Agrawal, A.; Shrivastav, R.; Satsangi, V. R.; Dass, S. A study on the photoelectrochemical properties of copper oxide thin films. *Int. J. Hydrogen Energy.* **2004**, *29* (2), 131−4.
(161) Gupta, M.; Sharma, V.; Shrivastava, J.; Solanki, A.; Singh, A. P.; Satsangi, V. R.; et al. Preparation and characterization of nanostructured ZnO thin films for photoelectrochemical splitting of water. *Bull. Mater. Sci.* **2009**, *32* (1), 23−30.
(162) Chandrasekaran, S. A novel single step synthesis, high efficiency and cost effective photovoltaic applications of oxidized copper nano particles. *Sol Energy Mater. Sol Cells.* **2013**, *109*, 220−6.
(163) Dimopoulos, T.; Peic, A.; Mullner, P.; Neuschitzer, M.; Resel, R.; Abermann, S.; Postl, M.; List, E. J. W.; Yakunin, S.; Heiss, W.; Bruckl, H. Photovoltaic properties of thin film heterojunctions with cupric oxide absorber. *J. Renew. Sustain. Energy* **2013**, *5*, 011205.
(164) Gao, F.; Liu, X. J.; Zhang, J. S.; Song, M. Z.; Li, N. Photovoltaic properties of the p-CuO/n-Si heterojunction prepared through reactive magnetron sputtering. *J. Appl. Phys.* **2012**, *111*, 084507.
(165) Lim, Y. F.; Choi, J. J.; Hanrath, T. Facile synthesis of colloidal CuO nanocrystals for light-harvesting applications. *J. Nanomater.* **2012**, *2012*, 393160.
(166) Wang, P.; Zhao, X.; Li, B. ZnO-coated CuO nanowire arrays: fabrications, optoelectronic properties, and photovoltaic applications. *Opt Express.* **2011**, *19* (12), 11271.
(167) Barreca, D.; Carraro, G.; Gasparotto, A.; Maccato, C.; Lebedev, O. I.; Parfenova, A.; et al. Tailored vapor-phase growth of CuxO-TiO2 (x = 1, 2) nanomaterials decorated with Au particles. *Langmuir.* **2011**, *27* (10), 6409−17.
(168) Barreca, D.; Carraro, G.; Comini, E.; Gasparotto, A.; MacCato, C.; Sada, C.; et al. Novel synthesis and gas sensing performances of CuO-TiO2 nanocomposites functionalized with Au nanoparticles. *J. Phys. Chem. C* **2011**, *115* (21), 10510−7.
(169) Duttaluru, G.; Singh, P.; Kumar Ansu, A.; kumar Sharma, R.; kumar, A.; Mishra, S. Methods to enhance the thermal properties of organic phase change materials: A review. *Mater. Today: Proc.* **2022**, *63*, 685−691.
(170) Gasparotto, A.; Barreca, D.; MacCato, C.; Tondello, E. Manufacturing of inorganic nanomaterials: Concepts and perspectives,. *Nanoscale.* **2012**, *4* (9), 2813−2825.
(171) Prasad, C.; Tang, H.; Liu, Q.; Bahadur, I.; Karlapudi, S.; Jiang, Y. A latest overview on photocatalytic application of g-C3N4 based nanostructured materials for hydrogen production,. *Int. J. Hydrogen Energy.* **2020**, *45* (1), 337−379.
(172) Vijaya, G.; Muralidhar, S. M.; Kumar, M.; Kumar, A.; Ashok Kumar, M.S.; Kumar, D.; Pandey, S.; Hasnain, S.M. M.; Singh, A. K.; Kumar, G. Nano Indentation Studies on Ceramic Thinfilms Coatings Deposited using Sputtering Process for Energy Applications. *Mater. Sci. Energy Technol.* **2024**, *7*, 115−123.
(173) Singh M, M.; Kumar, M.; Sivaiah, P.; G, V.; Kumar, A.; Kumar, D.; Pandey, S.; Singh, A. K.; Deifalla, A. F.; Hasnain, S.M. M. Simulation of metal ceramic single layer coatings for solar energy applications. *Mater. Sci. Energy Technol.* **2024**, *7*, 85−90.
(174) Kumar, A.; Layek, A. Effect of heat transfer and pressure drop characteristics on the performance analysis of an artificially roughened solar air heater. *Heat and Mass Transfer* **2023**, *59*, 891−907.
(175) Kumar, A.; Layek, A. Heat transfer measurement in a rectangular channel of solar air heater with winglet-type ribs using liquid crystal thermography. *J. Therm. Sci. Eng. Appl.* **2022**, *14* (4), 041006.
(176) Ganeshkumar, S.; Kumar, A.; Maniraj, J.; Suresh Babu, Y.; Ansu, A. K.; Goyal, A.; Kareem Kadhim, I.; Saxena, K. K.; Prakash, C.; Altuijri, R.; Ijaz Khan, M.; Hassan, A. M Exploring the Potential of Nano Technology: A Review of Nano-Scale Multi-Layered-Composite Coatings for Cutting Tool Performance. *Arabian J. Chem.* **2023**, *16*, No. 105173.
(177) Kumar, R.; Singh, B. K.; Kumar, A.; Ansu, A. K.; Goyal, A.; Saxena, K. K.; Gupta, M.; Agarwal, M. K. Design of water distribution pipes alongside modeling and simulation of water distribution system for efficient management. *Int. J. Interact. Des. Manuf.* **2023**, DOI: 10.1007/s12008-023-01436-z.
(178) Wu, X.; Chen, F.; Wang, X.; Yu, H. In situ one-step hydrothermal synthesis of oxygen-containing groups-modified g-C 3 N 4 for the improved photocatalytic H 2 -evolution performance. *Appl. Surf. Sci.* **2018**, *427*, 645−53.
(179) Kumar, S.; Reddy, N. L.; Kumar, A.; Shankar, M. V.; Krishnan, V. Two dimensional N-doped ZnO-graphitic carbon nitride nanosheets heterojunctions with enhanced photocatalytic hydrogen evolution. *Int. J. Hydrogen Energy* **2018**, *43* (8), 3988−4002.
(180) Sun, K.; Shen, J.; Liu, Q.; Tang, H.; Zhang, M.; Zulfiqar, S.; et al. Synergistic effect of Co(II)-hole and Pt-electron cocatalysts for enhanced photocatalytic hydrogen evolution performance of P-doped g-C3N4. *Chinese J. Catal.* **2020**, *41* (1), 72−81.
(181) Zhou, Y.; Zhang, L.; Liu, J.; Fan, X.; Wang, B.; Wang, M.; et al. Brand new P-doped g-C3N4: Enhanced photocatalytic activity for H2 evolution and Rhodamine B degradation under visible light. *J. Mater. Chem. A* **2015**, *3* (7), 3862−7.

https://doi.org/10.1021/acsomega.3c07822
ACS Omega 2024, 9, 6147−6164

(182) Wu, M.; Yan, J. M.; Tang, X. N.; Zhao, M.; Jiang, Q. Synthesis of Potassium-Modified Graphitic Carbon Nitride with High Photocatalytic Activity for Hydrogen Evolution. *ChemSusChem.* **2014**, *7* (9), 2654−8.
(183) Kumar, V.; Singh, N.; Jana, S.; Rout, S. K.; Dey, R. K.; Singh, G. P. Surface polar charge induced Ni loaded CdS heterostructure nanorod for efficient photo-catalytic hydrogen evolution. *Int. J. Hydrogen Energy.* **2021**, *46* (30), 16373−86.
(184) Higashi, T.; Shinohara, Y.; Ohnishi, A.; Liu, J.; Ueda, K.; Okamura, S.; et al. Sunlight-Driven Overall Water Splitting by the Combination of Surface-Modified La5Ti2Cu0.9Ag0.1S5O7 and BaTaO2N Photoelectrodes. *ChemPhotoChem.* **2017**, *1* (5), 167−72.
(185) Nandy, S.; Goto, Y.; Hisatomi, T.; Moriya, Y.; Minegishi, T.; Katayama, M.; et al. Synthesis and Photocatalytic Activity of La5Ti2Cu(S1−xSex)5O7 Solid Solutions for H2 Production under Visible Light Irradiation. *ChemPhotoChem.* **2017**, *1* (6), 265−72.
(186) Zhong, Y.; Li, Z.; Zhao, X.; Fang, T.; Huang, H.; Qian, Q.; et al. Enhanced Water-Splitting Performance of Perovskite SrTaO2N Photoanode Film through Ameliorating Interparticle Charge Transport. *Adv. Funct Mater.* **2016**, *26* (39), 7156−63.
(187) Sun, S.; Hisatomi, T.; Wang, Q.; Chen, S.; Ma, G.; Liu, J.; et al. Efficient Redox-Mediator-Free Z-Scheme Water Splitting Employing Oxysulfide Photocatalysts under Visible Light. *ACS Catal.* **2018**, *8* (3), 1690−6.
(188) Akhundi, A.; Zaker Moshfegh, A.; Habibi-Yangjeh, A.; Sillanpää, M. Simultaneous Dual-Functional Photocatalysis by g-C3N4-Based Nanostructures. *ACS ES T Eng.* **2022**, *2* (4), 564−85.
(189) Wang, X.; Sayed, M.; Ruzimuradov, O.; Zhang, J.; Fan, Y.; Li, X.; et al. A review of step-scheme photocatalysts. *Appl. Mater. Today [Internet]* **2022**, *29* (May), No. 101609.
(190) Tu, C. Y.; Wu, J. M. Localized surface plasmon resonance coupling with piezophototronic effect for enhancing hydrogen evolution reaction with Au@MoS2 nanoflowers. *Nano Energy [Internet].* **2021**, *87* (April), No. 106131.
(191) Yang, J.; Yan, H.; Wang, X.; Wen, F.; Wang, Z.; Fan, D.; et al. Roles of cocatalysts in Pt-PdS/CdS with exceptionally high quantum efficiency for photocatalytic hydrogen production. *J. Catal. [Internet]* **2012**, *290*, 151−7.
(192) Yang, J.; Wang, D.; Han, H.; Li, C. Roles of Cocatalysts in Photocatalysis and Photoelectrocatalysis. *Acc. Chem. Res.* **2013**, *46* (8), 1900−1909.

https://doi.org/10.1021/acsomega.3c07822
ACS Omega 2024, 9, 6147−6164